LAWRENCE
LIVERMORE
NATIONAL
LABORATORY

LLNL-TR-663757

Final LDRD Report for 12-ER-043: A New Approach for Reducing Uncertainty in Biospheric CO2 Flux

S. Wharton, M. Falk, J. Osuna, D. Baldocchi, K. Bible, S. Ma, J. Newman, R. D. Pyles, M. Schroeder

November 5, 2014

Disclaimer

This work performed under the auspices of the U.S. Department of Energy by Lawrence Livermore National Laboratory under Contract DE-AC52-07NA27344.

Final LDRD Report for 12-ER-043

A New Approach for Reducing Uncertainty in Biospheric CO_2 Flux

Primary Investigator
Sonia Wharton, Research Scientist, Lawrence Livermore National Laboratory

Co-investigators
Matthias Falk, Research Specialist, University of California, Davis
Jessica Osuna, Post-Doctorate Scholar, Lawrence Livermore National Laboratory

Collaborators
Dennis Baldocchi, Professor, University of California, Berkeley
Ken Bible, Wind River Field Station Director, University of Washington, Seattle
Siyan Ma, Research Specialist, University of California, Berkeley
Jennifer Newman, Ph.D. Candidate, University of Oklahoma, Norman
R. Dave Pyles, Research Specialist, University of California, Davis
Matt Schroeder, Site Technician, Wind River Field Station

November 1, 2014

LLNL-TR-663757

Table of Contents

Chapter 1: Introduction

In the 2010 Global Carbon Project Report it was estimated that the terrestrial biosphere sequesters 2.4 Pg of anthropogenic carbon emissions per year (Global Carbon Project 2010) although the uncertainty on that value is undoubtedly high as no error bars were given. As man-made emissions of CO_2 continue to increase unabated in the atmosphere, quantifying the fate of these anthropogenic sources requires both knowing the magnitude and uncertainty of background, natural CO_2 fluxes. Thus, reducing uncertainty in biospheric CO_2 flux measurements will not only give us direct, accurate observations for future carbon accounting and climate treaties but also indirectly help us quantify anthropogenic emissions for the same purposes. In conjuncture with ecosystem models or remote-sensing techniques, these measurements also provide accurate constraints on global and continental terrestrial CO_2 budgets.

Our understanding of biospheric CO_2 fluxes comes primarily from flux towers which measure CO_2, H_2O, and energy exchange between the vegetated surface and atmosphere with the eddy covariance (EC) technique. The proliferation of flux towers began in the late 1990's - early 2000's with towers rapidly erected in the U.S., Canada, Europe, Australia, and New Zealand (Baldocchi 2008). Today there are over 550 active flux sites across the globe, as part of FLUXNET, spanning nearly all biomes and climate zones, including more recent deployments in Mexico, South America, Asia, and Africa (Figure 1).

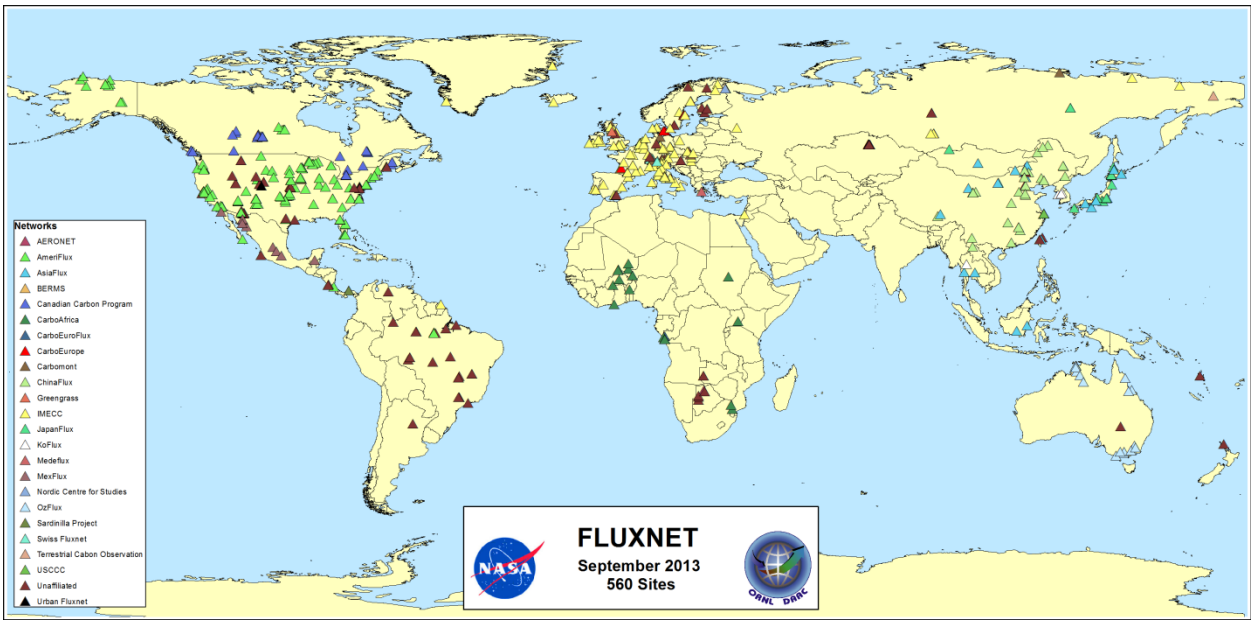

Figure 1: Map showing the current locations of biospheric CO_2 flux towers in the global FLUXNET network including symbols for the regional networks (ORNL DAAC 2013).

Given that hundreds of towers across the globe directly measure biospheric CO_2 exchange, the question then becomes, why is uncertainty in the land CO_2 flux so high? The simple answer is that the eddy covariance technique is imperfect. Flux towers suffer from logistical problems including instrument failure which lead to data gaps as well as from random and systematic errors inherit to the EC technique: rain, lack of turbulence, inhomogeneous terrain and vegetation lead to erroneous flux measurements. An example of this is shown in Figure 2. These periods of missing or erroneous data must be replaced with a gap-filling technique in order to estimate whether an ecosystem is a net annual carbon sink or source.

Current gap-filling methods are largely inadequate and over the course of a year, cause an average flux site to have an uncertainty of 25-50 g C m^{-2} yr^{-1} (Moffat et al. 2007, Baldocchi 2008). For an ecosystem that is a small annual sink or source of carbon (typical for a disturbed forest, grassland, or savannah ecosystem), this uncertainty is of the same magnitude as the measured flux.

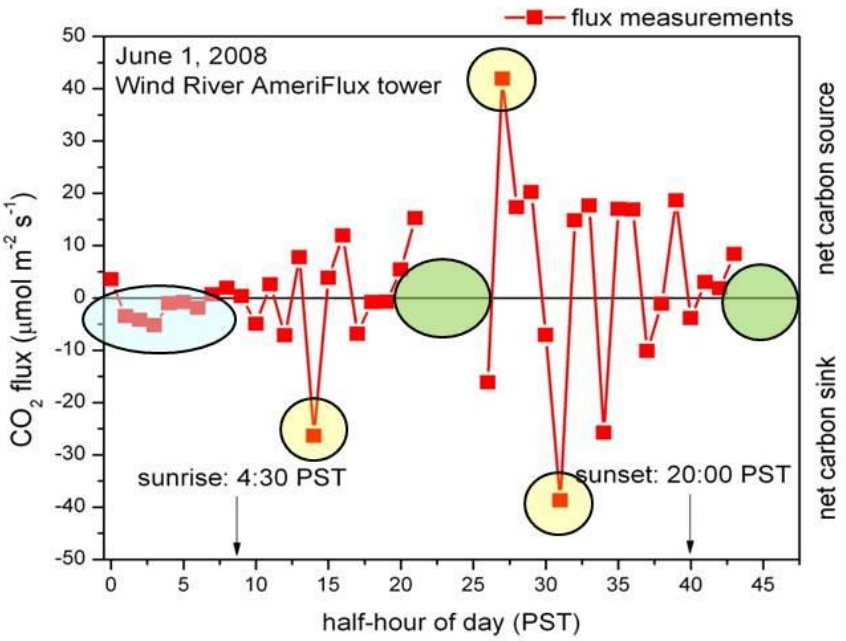

Figure 2: 30-minute CO_2 fluxes on a random day at Wind River reveal common errors and uncertainties associated with the eddy covariance measurement technique. Here, erroneous nighttime CO_2 fluxes are highlighted in blue, significant outliers are highlighted in yellow, and missing measurements due to a spike-filter removal are highlighted in green.

With the motivation stated above, we designed and executed a three-year Laboratory Directed Research and Development (LDRD) project with the aim of reducing the uncertainty in eddy-covariance biospheric CO_2 flux. Reducing uncertainty was approached in two ways. The first utilized nontraditional eddy covariance instrumentation to identify and characterize atmospheric flows above and within the plant canopy. Here, atmospheric laser detection and ranging (lidar) instrumentation were used to capture unique flow features at night which may explain erroneous or anomalous carbon fluxes (e.g, those highlighted in blue in Figure 2 which incorrectly indicate photosynthesis). The second approach utilized a multi-layer, 3rd order closure canopy-atmosphere model to simulate fluxes at each field site.

Three sites were chosen for field instrument deployment and modeling. These included the Wind River AmeriFlux tower in Washington State and the Tonzi AmeriFlux and Diablo AmeriFlux towers in northern California. These sites represent some of the extremes in the biological and meteorological conditions over which eddy covariance techniques are used. Wind River is a multi-layered, 60-m tall seasonal rainforest, Diablo is a 1-m tall grassland with a very short growing season, and Tonzi is a 2-layered savannah canopy with complex ecohydrology. All three are surrounded by complex terrain in varying degrees. The towers provided very different test sites for validating the UC Davis Advanced Canopy Atmosphere Soil Algorithm (ACASA) model. Such validation gives promise that the model can

be used to independently verify and gap-fill biospheric CO_2 measurements from the network of ~ 550 global flux towers for future greenhouse gas emissions monitoring and verification studies.

This report is organized in the following manner. Chapter 2 describes the three field sites and includes an introduction to Diablo, one of the newest AmeriFlux towers in the U.S. network. Chapter 3 describes the field instrumentation including the nontraditional use of atmospheric lidar and radiosonde technology in flux studies. Chapter 4 describes the results from our lidar-surface layer flows experiments for interpreting anomalous CO_2 fluxes. Chapter 5 describes ACASA and our modifications to the code. Chapter 6 describes the model simulations of carbon, water and energy fluxes with full validation. Chapter 7 provides conclusions from the project. Chapter 8 gives a list of presentations, manuscripts and author contributions. Chapter 9 is a list of references cited.

Chapter 2: Field Sites

2.1 Overview

The Diablo, Tonzi and Wind River AmeriFlux towers are geographically separated along a strong climate gradient found on the Pacific West Coast, U.S.A. (Figure 3). Here, precipitation is generally greater from north to south, from west to east, and on the western slopes of mountain ranges and large hills. Temperature follows a similar gradient with the northern and coastal areas having cooler annual temperatures and smaller temperature ranges. Very warm summer temperatures are common in the far inland areas. These gradients are illustrated by the range of annual precipitation and annual temperatures found at the three field sites. Annual precipitation (PPT) ranges in over 2 m between the driest site, Diablo, and the wettest, Wind River. Annual temperature (T_a) at Tonzi is nearly twice that found at Wind River. All three locations experience a seasonal wet-dry climate with the bulk of precipitation falling during the cooler November-March months.

Figure 3: Site map and description for the three AmeriFlux sites: Tonzi, Diablo, and Wind River. These locations cover a wide range of climatology from wet, cool conditions at Wind River to warm, very dry conditions at Diablo. Large differences in vegetation are a manifestation of climate. At Tonzi and Diablo, vegetation differences are also due to differences in sub-ground hydrology.

2.2 Diablo AmeriFlux

The Diablo AmeriFlux tower is located at Lawrence Livermore National Laboratory's Site 300 in the Altamont Hills in northern California, USA (37.677, -121.5296, 320 m a.s.l.). The tower was erected in October 2010 and established as an official AmeriFlux site in January 2013 under this LDRD. More information about the eddy covariance measurements are found in Chapter 3. Cool-season C3 grasses dominate the landscape and include slender wild oat (*Avena barbata*), ripgut brome (*Bromus diandrus*), soft chess (*Bromus hordeaceus*), and red brome (*Bromus madritensis*). The area has not been grazed

since 1953. Maximum rooting depth is 1.5 m (*Avena barbata*) with 70% of all grass roots within 0.15-0.20 m. The water table depth is deep and is well beyond the maximum rooting depth. In 2010, the water table averaged 24 m with very little seasonal variability (Dibley et al. 2011).

The site has mild, rainy winters and warm-to-hot, dry summers with just 20% of annual precipitation falling from April-October. Historical (1981-2010) mean annual temperature is 15.0 °C and mean water-year (October-September) precipitation is 265 mm (Jones et al. 2012). The growing season lasts approximately from November-late May although this varies considerably depending on the intensity and timing of rainfall. Maximum canopy height (h_c) and leaf area index (LAI) usually occur in mid to late April, however, peak values were reached in mid-March in 2013 (LAI_{max} = 1.6 m^2 m^{-2}; h_{cmax} = 0.70 m). LAI was measured at a semi-weekly frequency during the 2012-2013 growing season. Total 2012-2013 precipitation was 211 mm with most of it falling from November-January.

The terrain to the south and southwest is complex with a series of hills and ridges in the Diablo Range extending tens of kilometers although the immediate fetch is flat in the northerly and westerly directions (slope < 4%). In the warm months, a thermal contrast between the cooler Pacific coast and warmer Central Valley synoptically induces an onshore flow of marine air. These westerlies are channeled and strengthened by large gaps in the Coastal Range including the Diablo Pass. Local drainage flows can occur at night and are caused by forced channeling of cooler, denser air through canyons in the surrounding Diablo Hills.

2.3 Tonzi AmeriFlux

The Tonzi AmeriFlux tower is located in the lower foothills of the Sierra Nevada, California, USA (38.4318, -120.9668) at an elevation of 177 m a.s.l. The study area is dominated by deciduous blue oaks (*Quercus douglasii*) which cover roughly 40% of the landscape with some interspersed Gray pines (*Pinus sabineana*). Average LAI for the tree canopy is 0.71 ± 0.41 m^2 m^{-2}, mean h_c is 9.41 ± 4.33 m, and average tree diameter at breast height (dbh) is 0.22 m (Baldocchi et al. 2010). The vegetation is highly clumped and has a clumping element index of 0.49 (Ryu et al. 2010). The understory and open meadows are dominated by cool-season C3 grasses (*Brachypodium distachyon, Hypochaeris glabra, Bromus madritensis*) which are grazed by cows in the winter and spring. The oak-grass savannah is a two-layered system: grasses dominate the ecosystem CO_2 fluxes in the wet winter, trees and grasses dominate in the spring after bud break (typically in March), and trees dominate the fluxes in the summer when moisture limitations kill the grasses. The site has a Mediterranean climate and is characterized by wet, mild winters and dry, hot summers. Mean annual temperature is 16.5 °C; mean annual precipitation is 562 mm. Further stand details are found in Baldocchi et al. (2004, 2006), Ma et al. (2007), and Kobayashi et al. (2012).

While the local fetch is relatively flat the terrain becomes increasingly complex in the easterly direction towards the Sierra Nevada. Differential heating between the Sacramento Valley and mountains creates frequent diurnal slope flows in the warmer months. These cross-valley winds produce upslope or anabatic winds from the west during the day and downslope or katabatic winds from the east overnight (Hayes et al. 1984). Overnight, these gravity-driven flows typically produce a jet with maximum velocity 5-15 m a.g.l. over sloping terrain (Yi et al. 2005, Whiteman and Zhong 2008, Choi et al. 2011). The height of this jet, however, increases with increasing downslope distance and a maximum velocity can occur many tens of meters above the surface further downfield. Synoptic-scale flows in the warm months are dominated by the Pacific High offshore which creates prevailing westerly winds.

2.4 Wind River AmeriFlux

The Wind River Field Station (formerly the Wind River Canopy Crane Research Facility) is located in a 500-hectare old-growth, evergreen needleleaf forest in southern Washington, USA (45.8205, -121.9519, 371 m a.s.l.). The stand has never been managed and is thought to have originated after a natural fire around the year 1500. The old-growth forest is dominated by Douglas-fir (*Pseudotsuga menziesii* (Mirbel) Franco) and western hemlock (*Tsuga heterophylla* (Raf.) Sarg). Stand density is approximately 427 trees per hectare, tree ages range from 0 to ~500 years (Shaw et al. 2004), and LAI estimates range from 8.2 to 9.2 m^2 m^{-2} with little seasonality (Thomas & Winner 2000, Parker et al. 2002). Mean canopy height is approximately 50 m. The climate is characterized by wet and mild winters interspersed with a strong, seasonal summer drought (Shaw et al. 2004). Historical mean annual air temperature is 8.8 ^{o}C and total water-year precipitation is 2338 mm, of which on average only 322 mm falls from July through October.

The old-growth stand and flux tower lie in the Wind River Valley. The tower has a fetch of ~1 km of homogenous vegetation in the westerly direction across relatively flat terrain (slope = 3.5%). The surrounding terrain, however, is complex and local topographical features that can influence air flow at the tower include Bunker Hill to the southeast and Trout Creek Hill to the northwest. Differential heating in the local valley and mountains creates along-axis, diurnal mountain-valley flows. These flows are characterized by a reversal of wind direction twice a day with upslope, up-valley flows during the daytime and downslope, down-valley flows at night. At the synoptic-scale, gap flows are prevalent in the region caused by pressure driven channeling in the Columbia River Gorge which strengthens the summer-time prevailing westerly winds.

Chapter 3: Instrumentation

3.1 Eddy Covariance

Half-hour fluxes of carbon dioxide (F_c) (μmol m^{-2} s^{-1}), water vapor (F_{H2O}) (mmol m^{-2} s^{-1}), latent energy (LE) (W m^{-2}), and sensible heat (H) (W m^{-2}) were measured continuously at all sites with the eddy covariance (EC) technique. Two of the three AmeriFlux sites have long records of continuous flux measurements: Wind River since 1998 (Falk et al. 2005, 2008, Wharton et al. 2012) and Tonzi since 2001 (Xu and Baldocchi 2003, Baldocchi et al. 2006, Ma et al. 2007). Flux measurements at Diablo began in October 2010. Full instrumentation and data processing details can be found in the above citations for Wind River and Tonzi. In brief, Tonzi has two flux towers: one in the subcanopy with instruments at 2 m a.g.l. ($z = 0.2\ h_c$) and one with instruments above the canopy (overstory) at a height of 23 m a.g.l ($z = 2.5\ h_c$). The subcanopy station measures fluxes from the grasses and soil. At Wind River EC measurements are taken approximately 15 m above the canopy at a height of 67 m ($z = 1.2\ h_c$). Details for Diablo are given below for the first time.

Instrumentation at Diablo includes an open-path infrared gas analyzer (IRGA) (CS150, Campbell Scientific, Inc., Logan, Utah), 3-D sonic anemometer (CSAT 3A, Campbell Scientific, Inc.), net radiometer (NR-LITE-L, Kipp & Zonen, Delft, The Netherlands), soil heat flux plates (HFT3-L, Campbell Scientific, Inc.), soil temperature probes (TCAV-L, Campbell Scientific), soil moisture probes (CS616-L, Campbell Scientific, Inc.), and an air temperature/relative humidity sensor (HMP45, Vaisala Oyj, Helsinki, Finland). Soil moisture is measured at an integrated depth of 0-30 cm in three locations, soil temperature is measured at 10, 15, 20 and 30 cm, and ground heat flux is measured at a depth of 25 cm in two replicates. Within a kilometer of the flux tower is a tipping bucket rain gauge (260-2500-12, NovaLynx Corporation, Grass Valley, California). All instruments except for the tipping bucket are powered by solar and battery power.

The 3-D sonic anemometer and IRGA sensor heads are separated horizontally by a distance of 8.5 cm with the IRGA placed downwind to reduce flow distortion. Both are deployed on a 3 m tall tripod tower at a height of 2.1 m and are mounted 1.4 m upwind of the tower on a horizontal boom. The boom and instruments face southwest and into the predominate wind direction. The net radiometer and air temperature/relative humidity probes are mounted on the same tower on individual booms facing south (radiometer) and east (temperature/RH) at 2.1 m a.g.l. The EC measurements are collected at a sampling rate of 10 Hz and archived using a CR3000 datalogger (Campbell Scientific, Inc.) and 1 GB datacard. All other meteorological data are collected and archived as 30-minute averages. All measurements were downloaded approximately every week by exchanging data cards in the field. 30-minute fluxes are calculated in real-time with Webb-Pearman-Leuning (WPL) density corrections (Webb et al. 1980) from the 10 Hz raw data using a Campbell Scientific flux code (version 2.99.01) to check flux values in the field. During post-processing the archived 10 Hz EC data were run through EddyPro (version 4.2.1, LI-COR, Lincoln, Nebraska, USA) by the Lawrence Berkeley National Laboratory's AmeriFlux Management Project to calculate the final 30-minute carbon, energy and water fluxes. This procedure included coordinate rotations to force the mean crosswind and vertical velocities to zero, WPL density corrections, and spectral corrections. The Diablo flux and meteorological data are archived and made publically available on the AmeriFlux database (http://ameriflux.ornl.gov/fullsiteinfo.php?sid=237).

3.2 Lidar deployments

High-resolution profiles of wind speed, direction and turbulence were measured with ground-based, vertically-profiling, Doppler laser detection and ranging (lidar) instruments at each site. Our primary instrument was the Wind Cube v2 (NRG Systems, Hinesburg, Vermont, USA and Leosphere, Orsay, France). The Wind Cube v2 was used in five field campaigns: Wind River in May 2012 and July-October 2013, Tonzi in April 2012 and September-November 2012, and Diablo in December-April 2013. In addition, a second lidar model, the ZephIR 300 (Natural Power, Campbell Scientific, Logan, Utah, USA and Natural Power, North Ledbury, UK) was used at Tonzi in April-May 2013. In total over 8300 hours of lidar measurements were collected during the six field campaigns. Photographs of selected campaigns are shown in Figure 4.

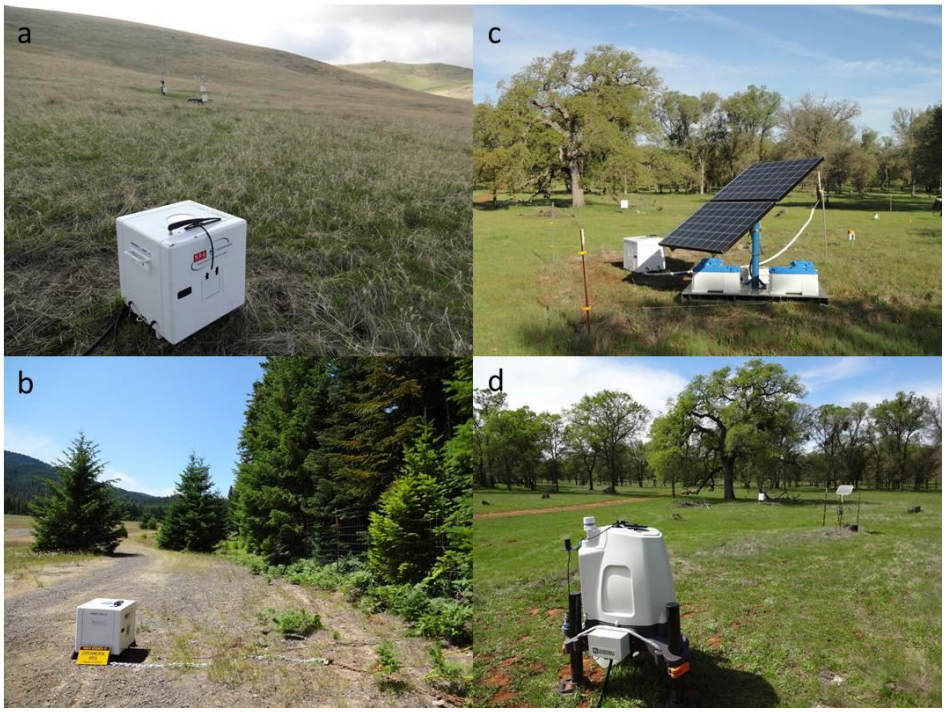

Figure 4: Photographs of lidar campaigns using the Wind Cube v2 at (a) Diablo, (b) Wind River, and (c) Tonzi. The ZephIR 300 was also used at Tonzi to take advantage of its ability to measure closer to the ground (d).

The Wind Cube v2 has the ability to measure 12 programmable heights across a 40-200 m a.g.l. maximum range. The ZephIR 300 in comparison measures 10 programmable heights across a wider maximum range (10-300 m a.g.l). At Diablo, we deployed the Wind Cube v2 40 m from the flux tower. At this grassland site, the minimum lidar measurement height (40 m) was well above the canopy height ($z = 55h_c$). At Wind River and Diablo we were hoping to sample measurements within the canopy as well as above. The average forest height at Wind River is at least 10 m above the Wind Cube's minimum measurement level ($z = 0.8\ h_c$); however, we were not able to find a gap large enough in the old-growth forest to prevent obstruction of the laser beams. Therefore, the lidar was placed in a clearing just outside of the forest and approximately 450 m south of the flux tower.

At Tonzi, the lidar was placed 110 m northwest of the flux tower. At this savannah site, large gaps between the trees allowed us to place the Wind Cube v2 directly within the canopy although the minimum measurement height was still well above the top of the canopy ($z = 4.2h_c$). To take advantage of the canopy gaps we acquired a ZephIR 300 lidar for use during the third campaign at Tonzi. The ZephIR 300 had a minimum measurement height near the top of the oak savannah canopy ($z \sim h_c$). This allowed us to examine flow characteristics in the canopy space between the subcanopy and overstory EC towers. The lidar at Tonzi and Diablo were powered by a combination of solar power and 12V batteries; at Wind River the lidar was powered by line power.

3.3 Lidar theory

Doppler lidar use laser radiation beams in the near infrared band to compute wind speed and wind direction from the radial component of the wind. A beam of radiation is emitted upward into the atmosphere by the instrument. If the beam illuminates an aerosol particle a small fraction of this light is backscattered to the lidar receiver. The motion of the aerosol along the beam direction leads to a change in the light's frequency via the Doppler shift. The "line-of-sight" velocity is measured from the Doppler-shifted light in the return signal assuming that the aerosols are moving in the same direction and at the same speed as the wind. Doppler wind lidar use either pulsed or continuous emission waveform. Here, we utilized both technologies.

The Wind Cube v2 is a pulsed lidar and uses regularly spaced emissions of light for a specified pulse length to measure the radial wind components using a Doppler Beam Swinging (DBS) technique (Strauch et al. 1984). The Wind Cube uses five beams, one in the vertical direction, and four around the zenithal directions (north, south, east and west) at a cone half-angle of 28° and a constant probe depth ($\Delta z = 20$ m) to derive the u, v, and w velocity components from the radial velocities. Measurements are taken from 40 m to 200 m at twelve user-defined heights at a sampling rate of approximately 0.25 Hz to complete a full DBS scan, however the Wind Cube actually calculates u, v, and w at a faster frequency (~1 Hz) using the current radial velocity and the radial velocity from the previous four beam locations (Cariou and Boquet 2010). All heights are measured simultaneously. The Wind Cube has an accuracy of ± 0.1 m/s for wind speed and 1.5° for wind direction in ideal conditions (e.g., stationarity conditions, flat terrain, homogenous flow). Additional details on the Wind Cube v2 are found in Cariou and Boquet (2010).

The ZephIR 300 is a continuous wave lidar and uses a multi-beam circular scan (1 scan per second, 50 measurements per scan, cone half-angle = 30°) (also called a VAD or velocity-azimuth display scan) to compute the wind speed and wind direction. Measurement levels are user-defined and limited to ten heights between 10 m and 300 m a.g.l. Probe depth (Δz) is not constant and increases with increasing height. Δz ranges from 1.4 m at 10 m a.g.l. to 15.4 m at 100 m. In ideal conditions, accuracy is < 0.5% for wind speed and < 0.5° for wind direction. Unlike the pulsed Wind Cube, each height is not measured simultaneously and instead is measured in series taking ~15 seconds to resample any given height. Further details can be found in Slinger and Harris (2012).

In our study, mean horizontal wind speed, vertical wind speed, wind direction, variance and turbulence kinetic energy (TKE) were computed as 30-minute averages using the high frequency u, v, and w data. While lidar provides measurements of turbulence it is important to note that these measurements may differ from those collected with a 3-D sonic anemometer. Lidar's larger sample volume, lower sampling frequency (especially in the case of the Wind Cube) and possible cross-contamination by the wind

components can lead to differences (Sathe et al. 2011). However, evidence is increasingly showing that while turbulence from a lidar is not exactly the same as measured by a 3-D sonic anemometer these remote sensing devices are able to capture energy scales across the lower-to-mid frequency end of the inertial subrange at many sites (e.g., Cañadillas et al. 2011, Newman et al. 2014).

3.4 Radiosondes

Three radiosonde campaigns were conducted during the course of the LDRD project. These included launches at Tonzi and Wind River in spring of 2012 and launches at Tonzi in autumn of 2012. A total of 42 radiosondes (DFM-06, GRAW Radiosondes GmbH & Co, Nürnberg, Germany) were successfully launched. Launch times were scheduled to maximize afternoon collection times but morning, evening, and nighttime launches were also made to study diurnal PBL development. Collected measurements included wind speed, direction, potential temperature, and humidity profiles within and above the planetary boundary layer (PBL) at a 1 Hz sampling frequency. These measurements were used to validate surface layer profile simulations of temperature and wind in ACASA. The potential temperature observations were also used to derive PBL height. While ACASA does not explicitly model boundary layer height when run in "single column mode" as we did here, the PBL heights were critical for understanding the development and behavior of the PBL under different surface energy regimes. Effects of drought and soil moisture on the surface energy balance and development and behavior of the PBL were of interest. Radiosonde campaign periods at Tonzi were chosen to highlight site hydrological and meteorological variability (Figure 5).

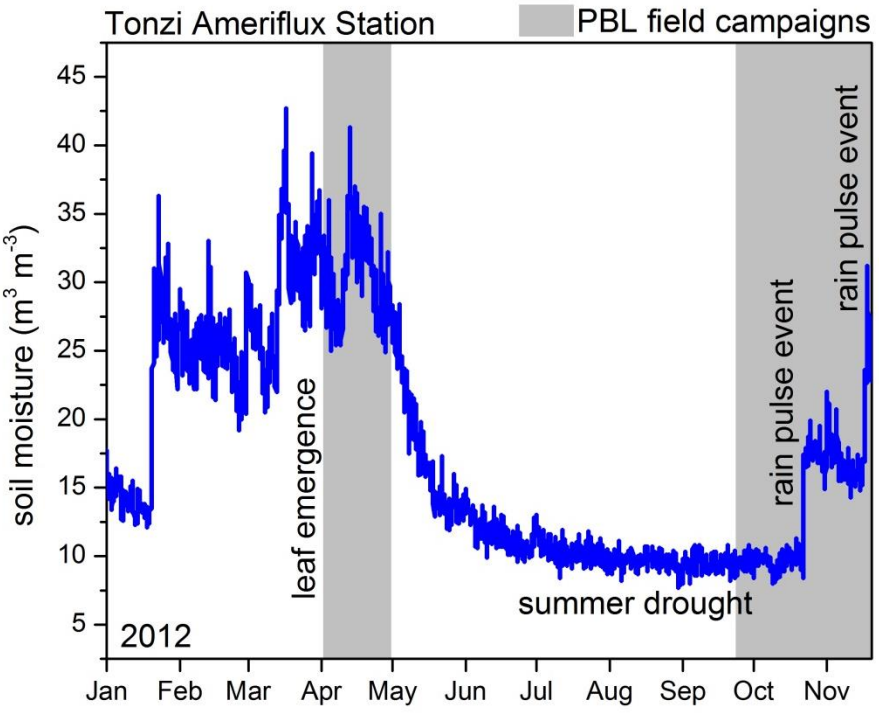

Figure 5: Time series of near-surface soil moisture data at Tonzi in 2012. These measurements show periods of spring moisture, summer drought, and significant rain pulse events in the autumn. Radiosonde campaigns (gray shaded regions) were chosen to highlight the hydrological differences on PBL behavior.

Radiosonde measurements for April 19 11:00 PST are shown in Figure 6 as an example of the data available for analysis. The campaign measurements at Tonzi showed a few surprises. First, the radiosondes showed that the maximum, spring-time PBL height occurs earlier in the day than expected. Second, while the maximum PBL height was lower following the rain pulse events (October), we did not also see lower maximum PBL heights during the moist spring (April) compared to the hot, dry summer (September) (Figure 7). Reasons for this unexpected finding should be further explored.

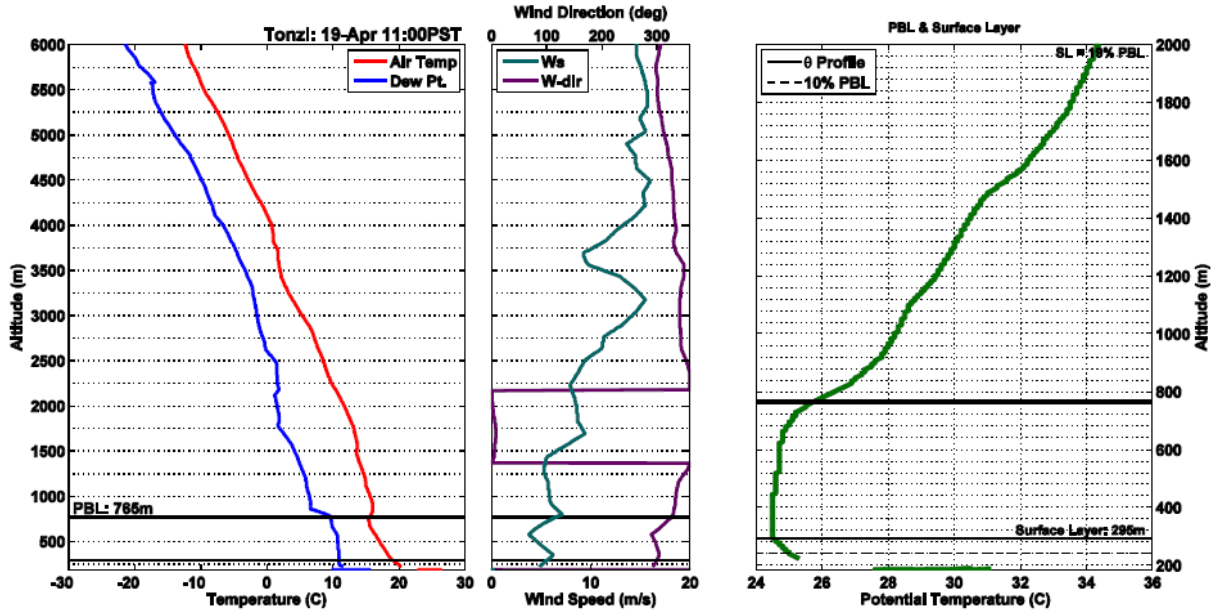

Figure 6: Radiosonde measurements taken at 11:00 PST on April 19, 2012 at Tonzi. Observations include vertical profiles of air temperature, dew point temperature, wind speed, wind direction, and potential temperature (θ). PBL height was derived from the temperature profiles using the parcel method. Surface layer height was estimated to be 10% of the PBL height.

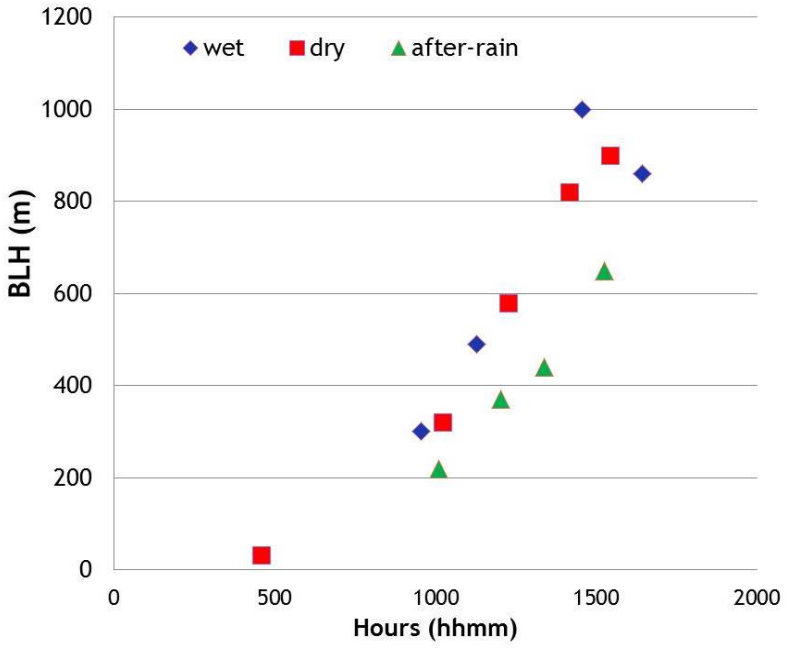

Figure 7: Planetary boundary layer height as a function of time of day for three days during the spring (wet), summer (dry), and autumn (after-rain) radiosonde campaigns at Tonzi. The after-rain maximum PBL height is lower than the dry season, as expected, while the maximum height during the wet spring period is higher than expected. Time is in local Pacific Standard Time.

The archived radiosonde data can be used in the future to validate a mesoscale model-ACASA simulation such as ACASA coupled to the Weather Forecasting and Research (WRF) model. Such simulations would allow high resolution modeling of surface energy exchange and carbon and water fluxes over larger spatial scales (> 1 km). Here, the radiosonde measurements would be used to validate model simulation of boundary layer development and height. Getting these conditions right is essential to accurately simulating flux exchanges over large spatial resolutions when the boundary layer is initialized by a mesoscale weather forecasting model. This methodology would potentially lead to more accurate predictions of regional-scale carbon, water and energy flux exchange than is currently available within WRF today.

Chapter 4: Lidar-Surface Flows Experiment for Assessing Flux Uncertainty

4.1 Introduction

Lower levels of the planetary boundary layer (PBL) tend towards stable conditions at night with turbulent transfer of mass and energy exchange driven solely by mechanically forced turbulence, either from frictional forces near the ground or at the top of the plant canopy or from "top-down" forced intermittent bursts of turbulence generated from wind shear aloft. The nighttime atmosphere is further complicated by variable topography which creates complex wind patterns near the surface including strong, along-valley-axis flows and gravity-driven downslope flows. These features challenge some of the major tenants of eddy covariance theory including the assumption of homogenous flat terrain and dominant vertical turbulence transfer. However, our need for understanding the terrestrial carbon budget requires that these types of measurements be made in places with non-ideal conditions.

Nighttime CO_2 flux data are most often quality-controlled using the momentum flux-derived variable friction velocity or ustar (also written as u_*) measured at the top or a few 10's of meters above the canopy. This method assumes is that there is a critical ustar value (u_{*crit}) beyond which the vertical transport of turbulence is adequate for the EC system to successfully measure accurate CO_2 fluxes. Fluxes which are determined to be measured during times of poor turbulent transport ($u_* < u_{*\,crit}$) are flagged and routinely replaced with modeled values based on an empirically-derived relationship between CO_2 flux and air temperature during high ustar conditions, and at water-limited sites, also with soil moisture. Limitations to the ustar correction method have been explored by others including Acevado et al. (2009), van Gorsel et al. (2009), and Wharton et al. (2009a). For instance, ustar taken just above the canopy may not be an accurate representation of turbulence conditions throughout the entire canopy, especially in dense canopies where flow decoupling frequently occurs and drainage flows in the subcanopy may be prevalent. Secondly, and perhaps more importantly for the wider FLUXNET community, ustar offers little to no insight into the drivers of turbulent processes which can originate well above or long distances from the tower measurements. Furthermore, Wharton et al. (2009a) argue that ustar is not an independent state variable when it is used to filter CO_2 fluxes because ustar is defined from the streamwise and crosswise momentum fluxes.

Within- and above-canopy atmospheric phenomena that may occur at flux tower sites and could be routinely missed by standard EC systems include but are not limited to low level jets (LLJ), gravity waves, katabatic flows, anabatic flows, other gravitational-induced subcanopy flows (e.g., drainage flows), and large-amplitude pressure waves (Durden et al. 2013). These phenomena are caused by a mixture of local scale (e.g., terrain, canopy structure) and mesoscale processes depending on the site and phenomena. Some of these features have been previously studied at FLUXNET towers including forested sites in British Columbia (Humphreys et al. 2003), Taiwan (El-Madany et al. 2014), Oregon (Vickers et al. 2012, Thomas et al. 2013), Colorado (Yi et al. 2005) and Florida (Karipot et al. 2006). Here, we will discuss two of those sites in more detail.

At the Campbell River FLUXNET site (British Columbia) relevant atmospheric phenomena result from a mixture of synoptic and local effects. For example, the prevailing summertime wind directions are a result of katabatic and anabatic flows caused by the northeast facing terrain (slope of 5-10°) and complementary land-sea circulation. This causes a distinct diurnal shift in wind direction whereby daytime winds are from

the east-northeast and nighttime winds are from the west-southwest. Implications for eddy covariance measurements include the under-measurement of nighttime carbon fluxes at the top of the forest canopy. During calm nights eddy fluxes of carbon dioxide are very small. These low values are likely due to mass flowing below the EC instruments as a result of cold air drainage flows down the slope. At the Florida AmeriFlux site mesoscale-driven low level jets introduce sporadic coupling between the forest canopy and atmosphere at night which influences the EC flux measurements. Although these jets are hundreds of meters above the canopy, turbulence is generated by shear just below the jet. This turbulence is able to periodically penetrate the canopy and stored CO_2 is vented out of the forest during these events. Without this inclusion of turbulence from LLJs stored CO_2 is routinely advected out of the system and missed by above canopy EC system resulting in an underestimation of nighttime respiration.

The occurrence and significance of distinct, above- and subcanopy atmospheric phenomena at these FLUXNET sites suggests that there may be limitations to our current way of instrumenting eddy covariance sites. This is especially true if above- or subcanopy flow phenomena are not infrequent or unusual but instead occur unnoticed at many flux towers. While this study can't answer that question for the entire flux network, we do investigate whether distinct atmospheric phenomena are common at three AmeriFlux towers in the Western U.S: Wind River, a tall, closed canopy forest; Tonzi, an open oak-grass savannah; and Diablo, a short grassland. Traditionally eddy covariance towers include little or no instrumentation 10s of meters or more above the canopy or within the subcanopy. In doing so certain atmospheric flows and phenomena are not measured and their potential impact on eddy covariance measurements is often ignored.

One possible way to measure above canopy and subcanopy flows at higher spatial resolution than has been previously done is to utilize laser detection and ranging (lidar) instrumentation. Lidars were first demonstrated in the 1970's (Jelalian 1992) and have since been applied to wide applications in aviation and meteorology. Over the last decade lidars have been routinely used to measure mean wind speed and wind profiles in the lower boundary layer (e.g., Smith et al. 2006, Pichugina et al. 2008, Peña et al. 2009, Wagner et al. 2009) These instruments have the advantage that they are highly mobile, relatively easy to deploy, and measure multiple heights up to 300 m above the ground level. Disadvantages of lidar include a minimum measuring height of 10 m which may be too high at many flux sites to capture subcanopy flows, lower temporal resolution as compared to sonic anemometers, and the need for open gaps within the canopy to allow for laser penetration of the atmosphere.

In this chapter we focus on using lidar to elucidate the importance of above-canopy flow features for identifying times and drivers of flux anomalies. Subcanopy flows are also briefly explored at the tree canopy sites, Wind River and Tonzi. Specific goals of were to: (1) identify atmospheric phenomena common to each site, (2) evaluate wind flow characteristics (e.g., shear, turbulence) at each site during strong and weak phenomena events, (3) identify anomalies or anomalous trends in the EC CO_2 flux record with emphasis on studying nighttime periods, and (4) identify any correlation between CO_2 flux anomalies and/or trends with the occurrence and strength of above-canopy atmospheric phenomena events. We also test the theory that above canopy-generated turbulence can significantly influence measurements of EC CO_2 fluxes.

4.2 Methods and Materials

Detailed site and instrument descriptions and experimental design are given in Chapters 2 and 3.

4.3 Results

4.3.1 Wind River

Lidar-observed atmospheric phenomena at Wind River included along-valley-axis, mountain-valley flow reversals, nights with very stable flows above the canopy, and nights with "top-down" forced turbulence produced above the canopy. The mountain-valley flow reversals were observed on 30% of the campaign days. An illustration of the mountain-valley flow is shown in Figure 8.

Figure 8: The mountain-valley flow reversal in the Wind River Valley, Washington. Northwesterly winds are common at night (blue arrow) and shift to the southeast during the day (yellow arrow). The Wind River AmeriFlux tower is indicated by the black star. The Columbia River is in the lower right.

An example of the lidar-measured flow reversals are shown in Figure 9. In addition to wind speed and direction, the multiple-level retrievals allowed us to observe wind shear, wind veer, and profiles of turbulence kinetic energy (TKE) above the canopy (Figures 9-11). At Wind River, nocturnal drainage flows were not observed with the lidar; however, they may have occurred undetected as the drainage flow was likely below the minimum measurement height (40 m). Significant wind veer was present when the winds aloft were from the northwest. This nighttime veer was caused by a clockwise rotation of the winds such that the flow was more northerly closer to the ground surface than aloft (Figure 9). Figure 10 shows a typical night with very stable nighttime flow above the canopy. During these events, the boundary layer above the forest had very low values of TKE, low wind speed, and low ustar (i.e., small momentum fluxes). Corresponding nighttime CO_2 fluxes were spikey and were often negative and indicated erroneous photosynthesis at night. Note the large CO_2 spike in the morning of 9/14 which corresponds with the transition from a stable nighttime boundary layer to a mixed daytime layer (Figure 10). Figure 11 shows a typical night with periodic "top-down" forced turbulence events. During these events, the boundary layer above the forest had very high values of TKE, wind shear and ustar. Corresponding nighttime CO_2 fluxes were small but largely positive in contrast to the negative fluxes measured during very stable nights.

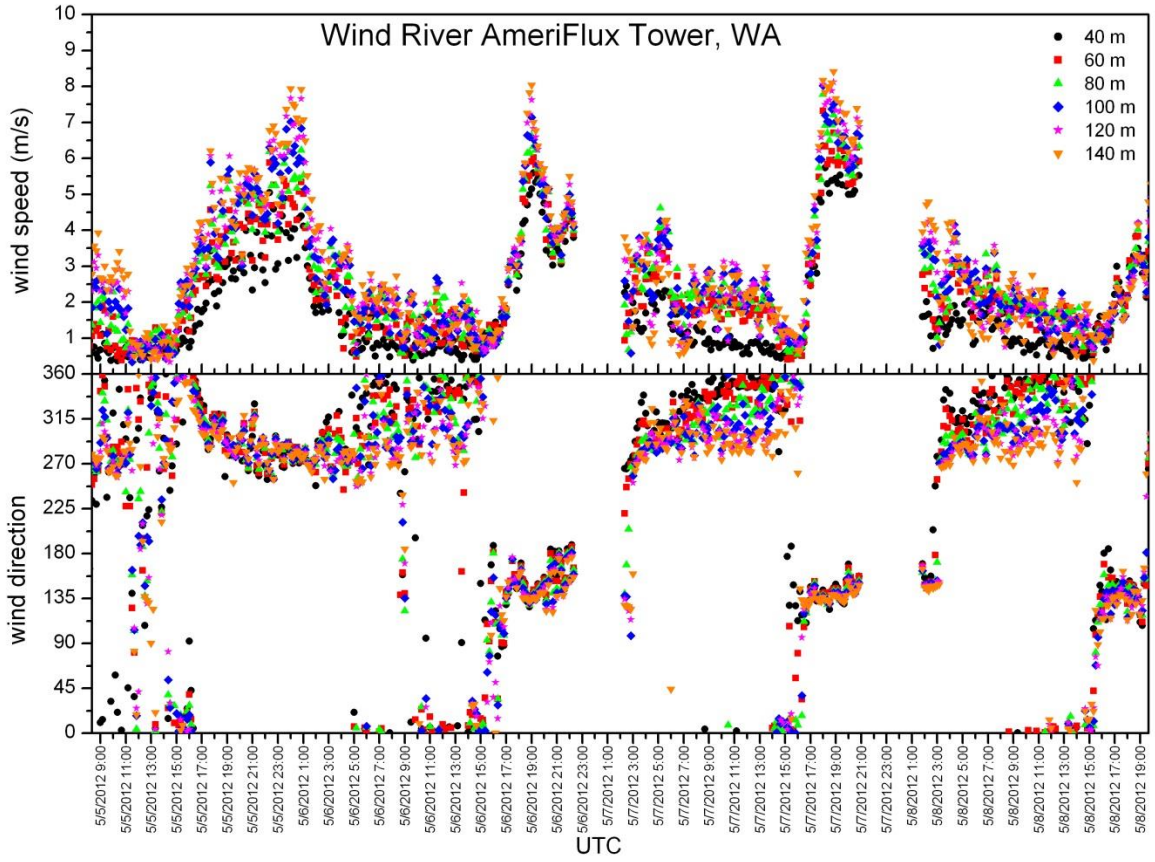

Figure 9: Lidar measurements of wind speed (top panel) and wind direction (lower panel) over three days in May 2012 at Wind River. The measurements show evidence of significant wind shear, rapid wind ramp events (i.e., sudden increases or decreases in wind speed), and flow reversals (i.e., shifts in direction from the northwest to southeast). The wind ramps were also associated with the sudden shifts in wind direction. Time is in Coordinated Universal Time (UTC).

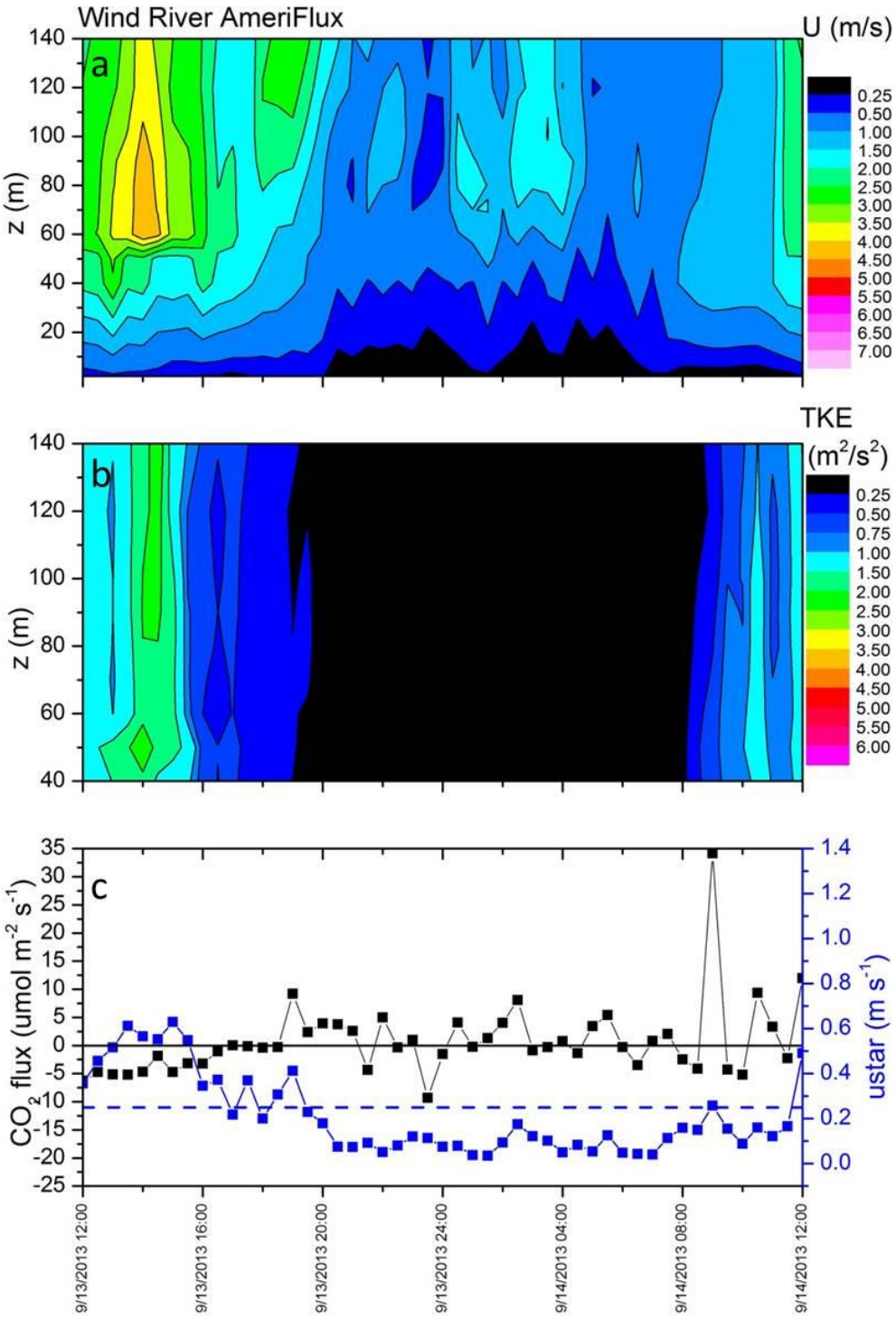

Figure 10: Contour plots of lidar (a) wind speed (U) and (b) turbulence kinetic energy (TKE) taken from 40-140 m. (c) Time series plot of EC CO_2 flux and ustar (i.e., friction velocity) taken at a height of 67 m. The data are plotted to highlight the nighttime period. 9/13-9/14/2013 is a typical example of nights that had a very stable boundary layer above the canopy. The dotted blue line indicates the site's ustar critical value. Time is in local Pacific Standard Time.

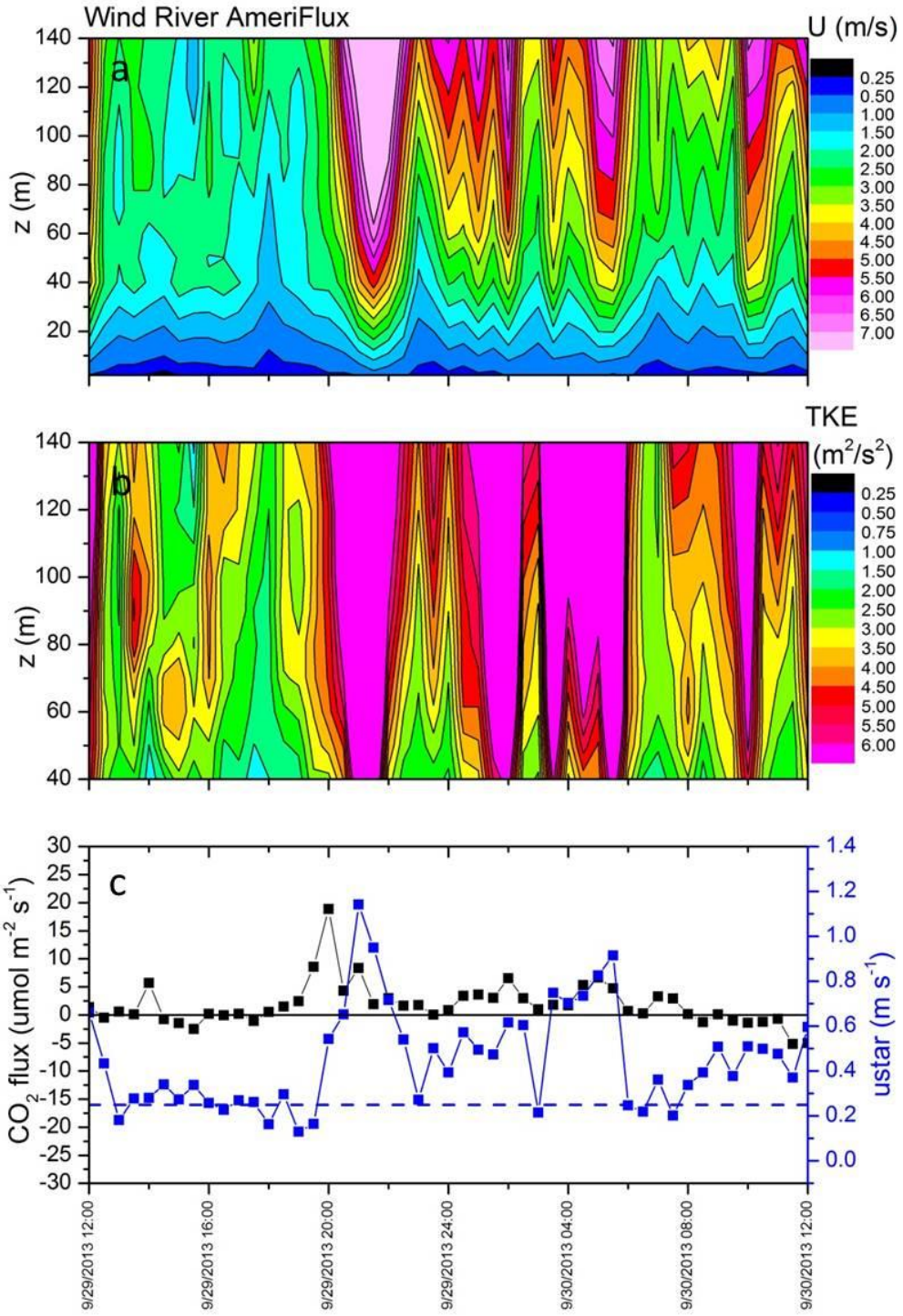

Figure 11: Same as Figure 10, except 9/29-9/30/2013 is plotted. This is a typical example of a night that experienced "top-down" forced turbulence events. The dotted blue line indicates the site's ustar critical value. Note the high correspondence between lidar TKE and EC ustar during these "top-down" forced events. Time is in local Pacific Standard Time.

Unfortunately we were not able to find a gap large enough in the forest canopy to allow for deploying the lidar within the forest. If we had been successful, the lidar would have provided subcanopy flow measurements. These measurements would have allowed for calculating how deep turbulence bursts penetrate the canopy during "top-down" forced turbulence events such as the one that occurred in Figure 11. With this in mind we looked at historic tower measurements at Wind River. From 1998-2006 wind speed, air temperature, relative humidity, and radiation measurements were taken along the 80-m tall tower at 10-20 m intervals. The historic vertical profiles of wind speed and direction show evidence of frequent subcanopy drainage flows at night. These are manifested through an observed secondary wind maxima in the canopy. The secondary wind maxima is found just below the height of maximum leaf area index (LAI) (Figure 12). These data are indicative of subcanopy flow decoupling although an analysis of the temperature profile would provide stronger definitive evidence.

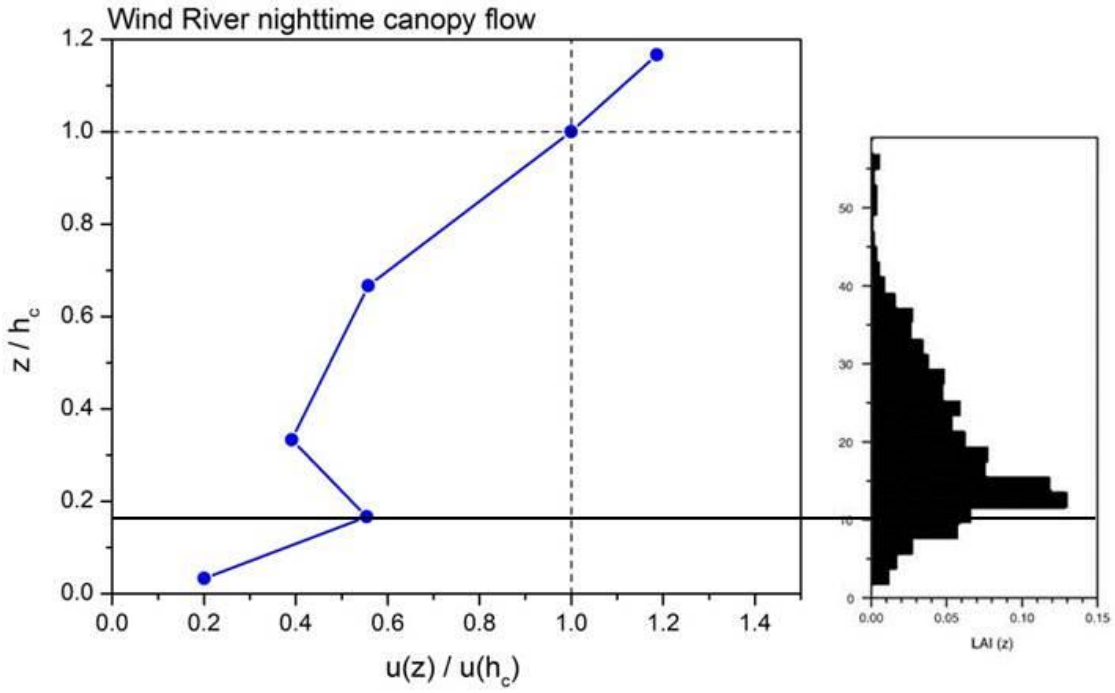

Figure 12: Normalized sonic anemometer wind speed data from 2003 at Wind River shows a secondary wind maxima occurring around 10 m a.g.l in the subcanopy. This maxima is likely due to a drainage flow and occurs just below the maximum LAI found at 15 m (right). Canopy height (h_c) here is 60 m.

4.3.2 Tonzi

Lidar-observed atmospheric phenomena at Tonzi included anabatic/katabatic slope winds, nights with "top-down" forced turbulence, and periods of strongly decoupled flow in the canopy. On 37% of the campaign nights katabatic flows were present over the site and created a shearing stress underneath the wind maximum. Although this height was typically well above the canopy (30-60 m a.g.l.), the jet sometimes developed at the same height or below the overstory eddy covariance system (z = 23 m). A topographic map showing the regional terrain and katabatic flow feature is shown in Figure 13.

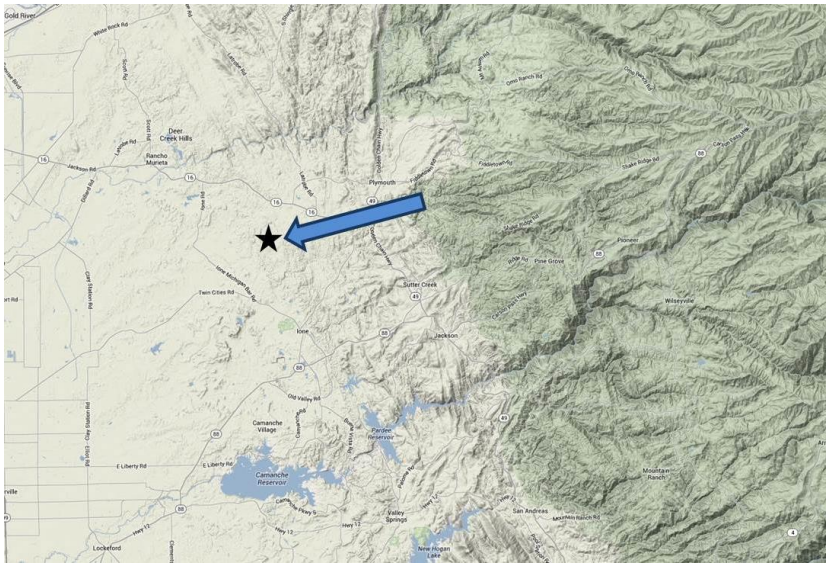

Figure 13: Topographic map of the region surrounding Tonzi (shown by black star). Although local fetch is relatively flat over one-third of the nights experienced katabatic slope flows from the east or northeast (blue arrow) due to regionally complex terrain in this direction.

The lidar allowed us to calculate the frequency of katabatic flows during the night and early morning hours at Tonzi (an example is shown in Figure 14). This was particularly meaningful when we utilized the ZephIR 300 lidar which had a minimum measuring height at 10 m which was near the top of the canopy. The understory EC system provided an additional data point closer to the surface (2 m) for quantifying whether the canopy was coupled or decoupled during these katabatic events.

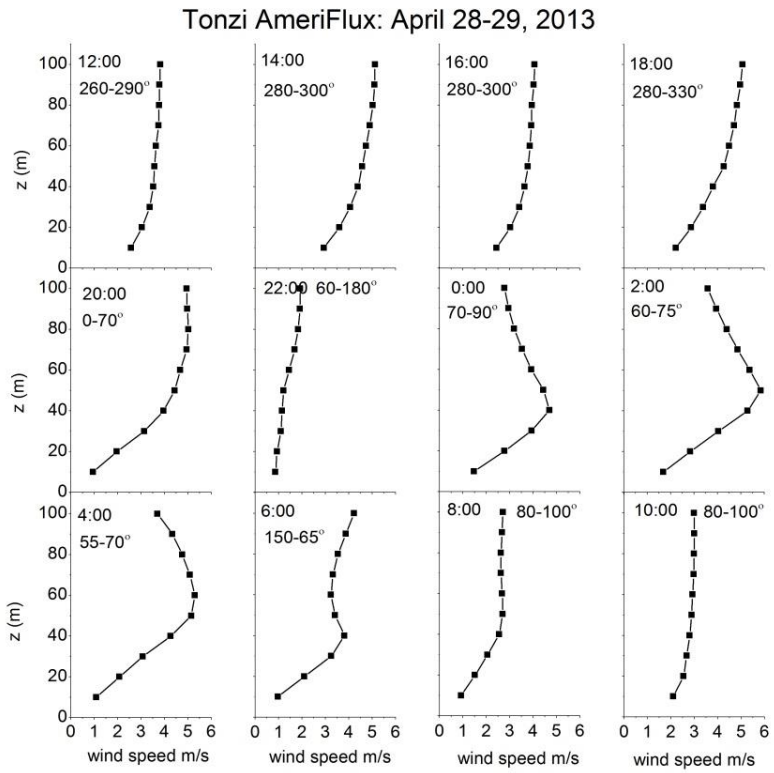

Figure 14: Vertical profiles of lidar wind speed at Tonzi show the emergence and progression of a katabatic flow on a night in April 2013. The jet is first observed over Tonzi at midnight and continues until the morning hours. The height of a wind jet maximum on this night varied from 40 to 50 m. The jet is associated with winds from the northeast on this night.

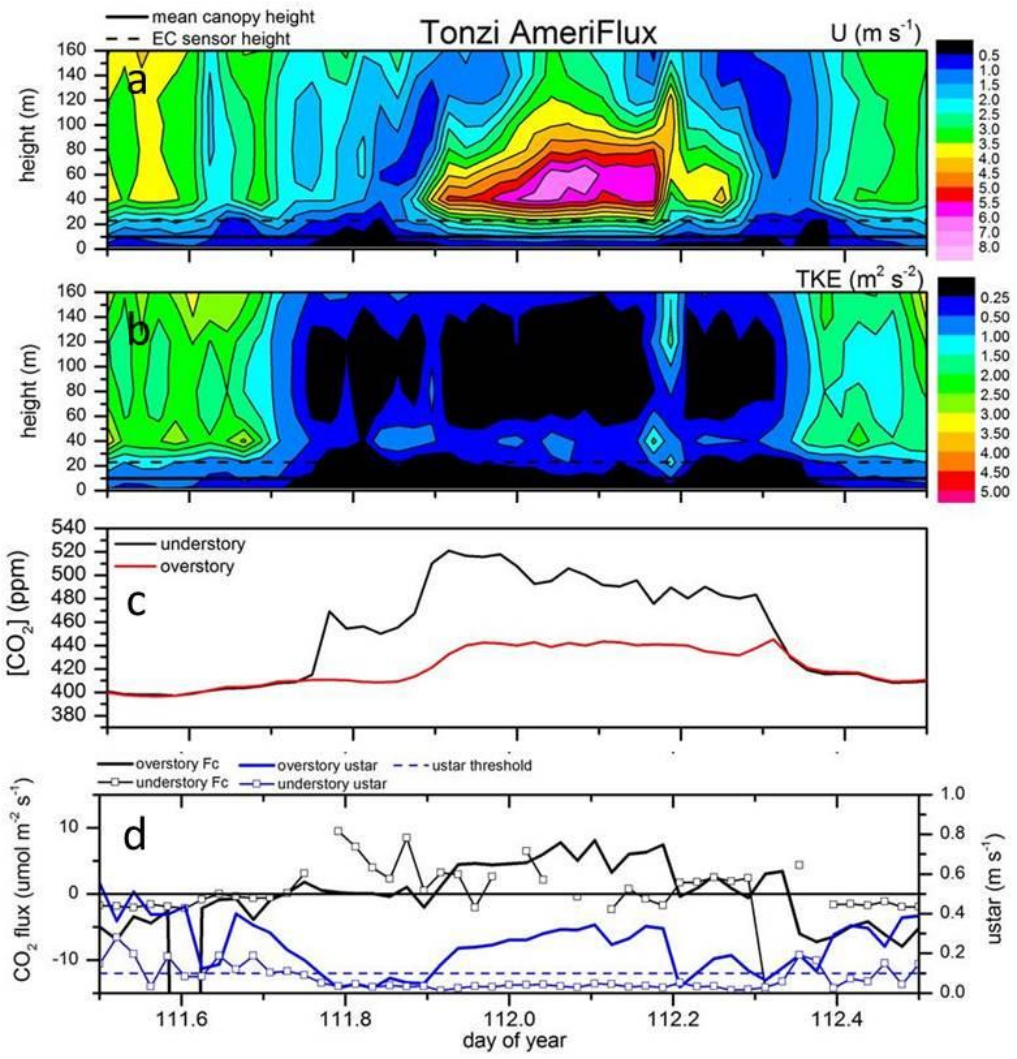

Figure 15: Plots of (a) lidar wind speed (U), (b) lidar turbulence kinetic energy (TKE), (c) eddy covariance CO_2 mixing ratio [CO_2], and (d) eddy covariance CO_2 flux and ustar at Tonzi from April 20-21, 2012. Note that the eddy covariance data show both the understory (2 m) and overstory (23 m) systems. This night clearly shows a strong katabatic flow with wind maximum around 40-60 m and strong canopy decoupling indicated by the large difference between [CO_2] at the top and bottom of the canopy.

For Tonzi we ran NOAA HYSPLIT back-trajectories for all nights to see if air masses during katabatic flows originated from different locations than non-katabatic flows. HYSPLIT assumes a 3-dimensional particle distribution to follow the advection of an atmospheric particle back in time to locate the origin of the air mass (Draxler and Hess 1997, Draxler and Rolph 2014). The model was run in back trajectory mode for 3 hours starting at 3:00 PST. The results showed that most of the katabatic flows, including the one shown in Figure 15 (April 20-21), originated from higher elevations in the Sierra northeast or east of Tonzi. The air mass on the night of April 16-17 (Figure 16), in contrast, originated from the south over the flat Central Valley. This flow was not indicative of a katabatic jet and instead showed a typical night with "top-down" forced turbulence.

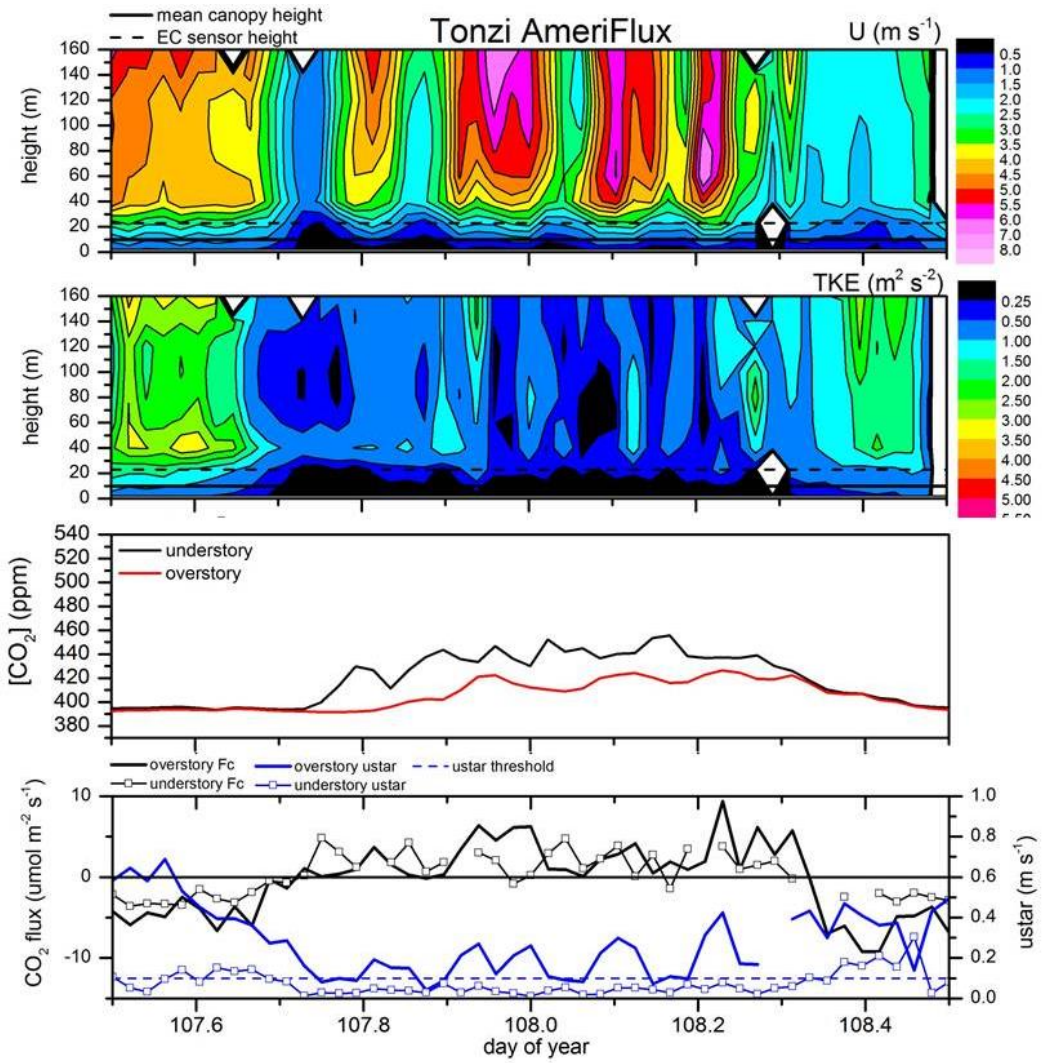

Figure 16: Same as Figure 15, except for April 16-17, 2012. This night shows intermittent "top-down" forced turbulence produced by high wind speeds and shear far above the canopy. The turbulent bursts periodically penetrate the canopy and flow within the canopy is more strongly coupled than during katabatic flow events. This increase in mixing is illustrated by smaller differences in [CO_2] between the top and bottom of the canopy.

Katabatic flows at Tonzi create a shearing stress just underneath the jet. This is seen in Figure 15 as elevated values in TKE are found below the wind speed maximum. Subsequently ustar is very high at the overstory EC and overstory CO_2 fluxes are largely positive indicating respiration, however the air just above the ground and in the subcanopy remains very stable. During this event, nocturnal drainage flows very close to the ground may be occurring and advecting CO_2-rich air out of the canopy. Although it is impossible to say this definitively as advection instrumentation are lacking, it is likely that the overstory EC system undermeasures ecosystem respiration during katabatic flow events given the evidence of flow decoupling and elevated [CO_2] at the 2 m station.

During katabatic flows it appeared that the shear-generated turbulence is not transported to the ground. However during "top-down" forced turbulence events, as shown in Figure 16, the intermittent transport of turbulence appears to be sometimes deeper creating mixing within canopy. Here, the differences between the understory and overstory CO_2 concentration and fluxes are smaller. This suggests that the overstory EC system is able to measure a greater portion of the total ecosystem respiration during "top-down" forced turbulence events than during katabatic flows.

4.3.3 Diablo

Lidar-observed atmospheric phenomena at Diablo included afternoon sea breezes, nights with local cold air drainage flows, and nights with "top-down" forced turbulence. We observed strong drainage flows on 23% of the springtime nights induced by a local terrain feature to the southwest (Figure 17). However, these drainage flows may be much more common and missed by our lidar system as the minimum measurement height was 40 m. Nighttime lidar profiles during observed drainage flows and non-drainage events are shown in Figure 18 with their associated wind directions. Here we can see a strong channeling of wind during drainage flow events. However, the lidar measured flow features at Diablo appear to not have a significant effect on 2-m EC measured CO_2 fluxes and ustar (Figure 19).

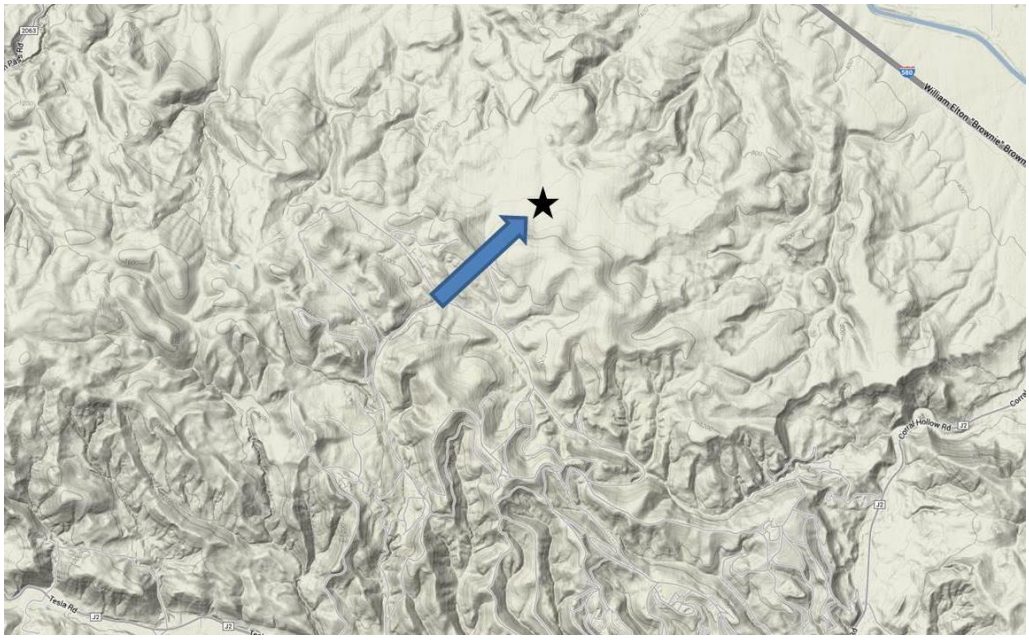

Figure 17: Topographic map showing the location of the Diablo AmeriFlux tower (black star) and local terrain features. Nocturnal drainage flows from the local canyon in the southwest (blue arrow) were observed with the lidar.

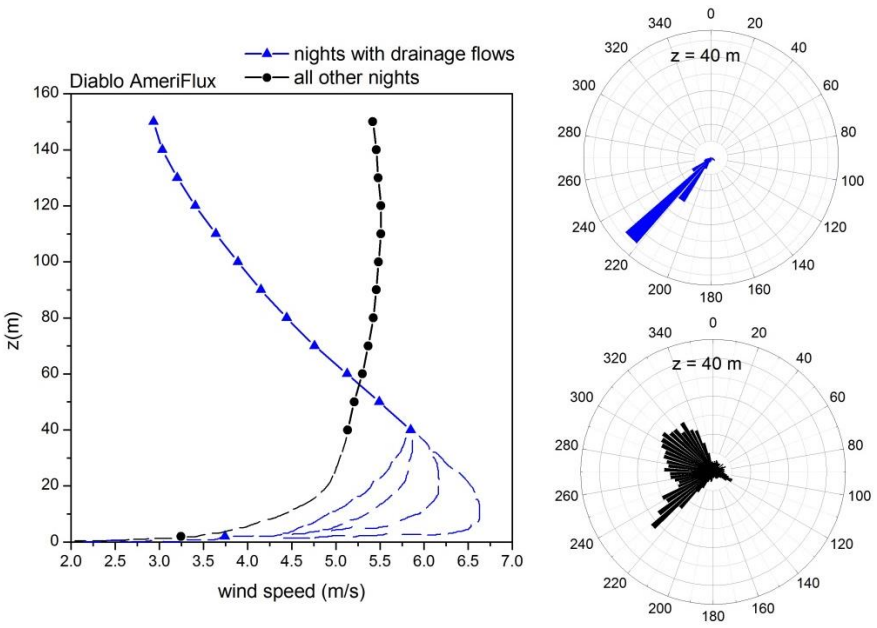

Figure 18: Mean wind speed profile during drainage flows (blue) and on all other nights (black) as measured by the lidar. The observations at 2 m are provided by the EC sonic anemometer. The profiles between 2-40 m are hypothesized (dashed lines) as measurements in this region are missing. The wind rose shows strongly channeled flow at 40 m from the southwest during the drainage events (top right).

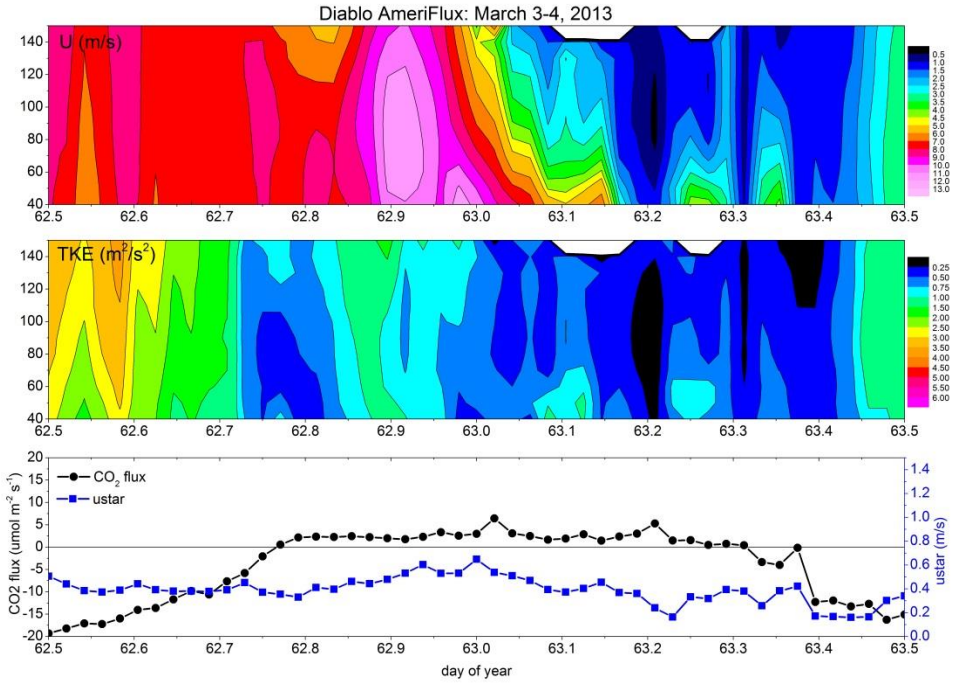

Figure 19: Plots of wind speed (U), turbulence kinetic energy (TKE), and EC CO_2 flux and ustar at Diablo on the night of March 3-4. This night shows evidence of a nocturnal drainage flow occurring around 2 am and lasting until 8 am. The height of the drainage flow varies and without measurements below 40 m it is impossible to know how shallow the flow maximum occurs.

4.4 Conclusions

At Diablo turbulence at night is usually sufficient for the eddy covariance method and we observed very few CO_2 flux anomalies or negative nighttime fluxes at this site. Although we observed drainage flows with the lidar, the EC fluxes appear to be unaltered by the presence of these flows and the Wind Cube v2 lidar was of little use for CO_2 interpretation for the short grassland canopy.

At Wind River we were unfortunately not able to deploy the lidar inside the forest canopy making it impossible to measure subcanopy flows and canopy penetration depth of "top-down" forced turbulence. Instead historic tower profile data showed that near-surface subcanopy flows are very common and the canopy is often decoupled at night. The lidar showed strong differences in wind speed and turbulence over the canopy as some nights experienced very stable flows above the canopy and to heights well above while other nights experienced higher wind speeds, higher shear, and "top-down" forced turbulence. However, EC CO_2 fluxes measured at the top of the canopy were not distinguishably different during these atmospheric events. This could be because "top-down" forced turbulence is not able to penetrate the closed, high LAI forest canopy although confirmation would require a combination of concurrent lidar and vertical profile tower measurements.

At Tonzi, the use of lidar is most promising for interpreting ecosystem flux anomalies as we saw evidence of turbulence penetrating deep into the open oak canopy. The lidar showed two mechanisms for producing nighttime turbulence – a shearing stress underneath katabatic flows and intermittent "top-down" forced turbulence. "Top-down" forced turbulence appeared to penetrate the canopy at deeper depths than the katabatic shearing stress leading to more mixing within the canopy and fewer CO_2 flux anomalies (e.g., negative nighttime fluxes occurred less frequently) than during other nighttime flows. The ZephIR 300 lidar was especially useful at Tonzi as it had a minimum measuring height of 10 m. The understory EC station at Tonzi also provided essential information for determining flow coupling or decoupling. Deploying a lidar at other suitable sites would provide more definitive answers for how important above-canopy, atmospheric-driven turbulence is for causing EC CO_2 flux anomalies and errors.

Chapter 5: New Modifications to ACASA

5.1 Model Background

Missing or erroneous data in flux tower records must be gap-filled in order to obtain annual sink/source estimates. Due to lack of turbulence at night (i.e., the mechanism which transports mass and energy from the ecosystem to the height of the sensors) most flux tower sites have to "correct" or gap-fill 50-80% of their nighttime data. This is often done using the empirical data relationships discussed in Chapter 4. Data gaps during the day must be gap-filled as well. Current methods range from the simplest, such as the mean diurnal averaging approach (Falge et al. 2001) to the more complex, such as artificial neural networks (Papale and Valentini 2003) or process-based models (e.g., Biome-BGC, Thornton et al. 2002). Process-based models typically rely on parameterizations of biogeochemical and ecophysiological processes with little attention made to above canopy atmospheric processes. We take a different approach here and test an advanced higher-order-closure-model. The goals were to (1) assess its accuracy in simulating energy, H_2O, and CO_2 fluxes and (2) assess under which conditions a higher-order-closure model is required. The Advanced Canopy-Atmosphere-Soil Algorithm (ACASA) model is a 3rd order closure model developed by the University of California, Davis (Figure 20).

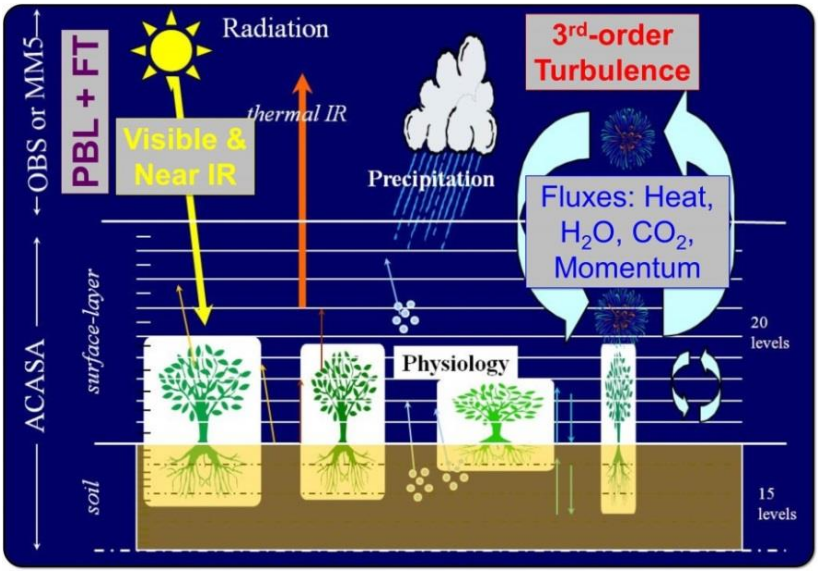

Figure 20: Schematic of the Advanced Canopy-Atmosphere-Soil Algorithm (ACASA) model. Instead of relying on a mesoscale model, site-measured values of CO_2 mixing ratio, air temperature, humidity, turbulence, and wind speed were used as model input. ACASA is more sophisticated than many other soil-vegetation-atmosphere transfer models with its multi-layer parameterization of subcanopy and above canopy turbulence.

ACASA uses fully diabatic, Reynolds-averaged equations closed at the third order for estimating turbulence and mass fluxes for each layer above the canopy (Pyles et al. 2000). It has advantages over simpler soil-vegetation-atmosphere transfer (SVAT) models (e.g., Mixfor, Olchev et al. 2008; MOSES, Harris et al. 2004; CLASS, Arain et al. 2002) which are unable to resolve vertical variations in wind velocity, air temperature, humidity, and CO_2 concentrations above the canopy. These profiles affect the physiological responses of the ecosystem to the microenvironment (Marras et al. 2011) and must be accurately parameterized in order to simulate CO_2 flux exchange with a high level of certainty.

5.2 Model Description

Turbulent transfer throughout the column is described by a diabatic, third-order closure method (Meyers and Paw U 1986). Surface temperatures are calculated using a near-exact quartic energy balance formulation producing accurate estimates even when components of the canopy have temperatures significantly different from ambient air temperature (Paw U and Gao 1988). Leaf-level photosynthesis is calculated for 10 different leaf-angle classes—including 1 shaded—via a combination of the Ball-Berry conductance method (Collatz et al. 1991) and the Farquhar-von Caemmerer-Berry model of CO_2 assimilation (Farquhar et al. 1980). Leaf absorption, reflection, transmission, and emission of both direct and diffuse radiation drive the energy fluxes in ACASA in addition to sensible and latent heat storage fluxes from the canopy.

ACASA's soil module is a diffusion-based model based on the NOAA-MAPS soil conduction and hydrology module (Smirnova et al. 2000) for both the soil and/or snow thermal and hydrological dynamics. The model can accommodate 4 - 15 layers in the soil (defined by the user) wherein temperature and moisture are calculated from initial conditions. ACASA distinguishes layers of the soil with and without roots present, as defined by the user.

For calculations of radiation, the canopy profile in ACASA is divided into 100 layers. For flux and turbulence calculations, the canopy is divided into 10 layers and the region from the top of the canopy to the top of the column (ideally at least twice the canopy height) is divided into 10 additional layers for a total of 20 layers of turbulence calculations.

The ACASA model is parameterized with information describing the physical characteristics of the canopy, soil properties and initial conditions, as well as radiative properties of the site (Table 1). The soil is classified based on a system of 21 soil classifications and then assigned properties based on this classification including values such as maximum and minimum soil moisture. Additionally, the user assigns the number of soil layers, the width of each layer, and the number of layers with active roots present. Soil moisture and temperature are used to produce the soil profile of each in the first timestep and then are calculated based on the soil module in ACASA.

The live canopy is parameterized using the green leaf area index (LAI), the vertical structure of the canopy, and the photosynthetic capacity of the dominant vegetation type. Canopy height and basal respiration are also used to parameterize ACASA. The reflectivities in the visible and near-infrared portion of the spectrum are assigned to each the canopy and the soil surface.

Well over 75 terrestrial biosphere models currently exist (Fisher et al. 2014), each with a different approach at simulating the land surface. The strengths of each vary based on history, purpose, and scale. One of the more generally used models, Biome-BGC (Running and Hunt 1993) is frequently cited in the literature for assessing site or regional carbon and water dynamics (e.g., Chiesi et al. 2007, Kang et al. 2014). Limitations to Biome-BGC include a single-layer canopy and daily time step. In the model, the biosphere responds to simple meteorological input such as maximum and minimum daily temperature, but there is no incorporation of feedbacks between the biosphere and the atmosphere. Biome-BGC has other strengths such as also simulating the nitrogen cycle at a site and simulating the phenology of a site rather than determining canopy state via parameterization. As such, it is useful for calculating long-term cumulative carbon or water fluxes, but cannot assess turbulent transfer above and throughout a complex

canopy. ACASA has a flexible time step and can be used to simulate fluxes at a temporal resolution that matches the measurements, allowing for the model to be used not just for ecosystem budgets but also for understanding the canopy-atmosphere feedbacks which drive fluxes.

CLM, or the Community Land Model is a land surface model specifically designed to be coupled with the Community Earth System Model (CESM) and the Community Atmosphere Model (CAM) (Bonan 1996). As opposed to Biome-BGC, CLM is designed explicitly for incorporating the coupling of the land surface and atmosphere into larger-spatial scaled climate simulations. CLM operates on a spatial scale equal to a grid cell in a Global Circulation Model (GCM). Subgrid variability allows for spatial heterogeneity in canopy type. CLM also permits the user to make simulations with a variety of configurations; for example, one can activate a dynamic vegetation model to make predictions of plant establishment and survival on long timescales (hundreds of years). Many recent advancements in CLM have focused on improving the hydrology of the model by connecting the soil water to groundwater (Niu et al. 2005) and to improve the snow dynamics (Flanner and Zender 2005, 2006, Flanner et al. 2007). Despite the complex hydrology and snow dynamics, CLM still operates with a single layer canopy for any plant functional type present in a grid cell. While it works well for coupling with a large scale GCM, it is not appropriate for simulating dynamics at a smaller spatial scale as ACASA does.

While our project ran ACASA in a stand-alone mode, ACASA, like CLM, has recently been coupled to the mesocale Weather Research and Forecasting (WRF) model to replace WRF's pre-existing land surface models (LSM) (e.g., Noah, RUC) (e.g., Falk et al. 2014, Xu et al. 2014). The WRF model, driven by North American Regional Reanalysis data (NCAR-NCEP) is run down to the planetary boundary layer, where ACASA is then called. Unlike existing LSMs in WRF, ACASA allows for microenvironmental variables such as air and surface temperatures, wind speed, humidity, and CO_2 concentration to vary vertically. ACASA also includes a realistic counter-gradient transport that low-order closure models are unable to simulate. Coupling ACASA to WRF bridged the gap between in-situ applications (e.g., AmeriFlux tower) and regional climate research with the sophistication of a 3rd order closure, multi-canopy model.

Table 1: Description of parameters and input required to use the ACASA model.

Variable	Description	Constant Parameter (P), Updated Parameter (UP), or Driving Input (DI)			
		V1	V2	V3	V4
zlatitude	Latitude of site	P	P	P	P
isoi3	Surface type (land, soil, water, ice, etc.)	P	P	P	P
smcdry9	Air dry value of soil moisture	P	P	P	P
smcref9	Reference value of volumetric soil moisture content	P	P	P	P
psisat9	Saturated soil moisture potential	P	P	P	P
bexp9	Clapp & Hornberger exponential B parameter	P	P	P	P
dksat9	Maximum hydraulic conductivity	P	P	P	P
smcmax9	Field capacity of the soil	P	P	P	P
nsoil0	Total number of soil layers	P	P	P	P
nroot	Total number of soil layers with active roots	P	P	P	P
ishallow	Flag to signal shallow-rooted vegetation is present	P	P	P	P
zs19	Soil layer width	P	P	P	P
zmoi	Wilting point soil moisture	P	P	P	P
tsinit	Initial soil temperature	P	P	UP	UP
qsinit	Initial soil moisture	P	P	UP	UP
xlai7	Total green leaf area index	P	DI	UP	UP
iveg	Canopy profile architecture	P	P		
xrsmn9	Photosynthetic capacity	P	P	P	UP
drx9	Mean canopy element drag coefficient	P	P	P	P
pv09	Maximum background PAR reflectivity	P	P	P	P
pr09	Maximum background near-infrared reflectivity	P	P	P	P
emissi8	Leaf (or surface) thermal emissivity	P	P	P	P
pv09g	Maximum ground PAR reflectivity	P	P	P	P
pr09g	Maximum ground near-infrared reflectivity	P	P	P	P
xldiam9	Mean leaf diameter	P	P	P	P
tr09	Mean near-infrared transmissivity	P	P	P	P
tv09	Mean visible transmissivity	P	P	P	P
r0r9	Basal Respiration rate, roots	P	P	P	P
r0m9	Basal respiration rate, microbes	P	P	P	P
r0s9	Basal respiration rate, soil	P	P	P	P
r0l0	Basal respiration rate, leaves	P	P	P	P
q10r9	Q10 of root respiration	P	P	P	P
q10m9	Q10 of microbial respiration	P	P	P	P
q10s9	Q10 of soil respiration	P	P	P	P
q10l9	Q10 of leaf respiration	P	P	P	P
standage	Canopy height	P	P	P	P
domain_height	Total ACASA domain height	P	P	P	P
Precipitation	Precipitation	D	DI	DI	DI

Humidity	Absolute humidity	D	DI	DI	DI
Wind_Speed	Wind speed	D	DI	DI	DI
Downward_shortwave_flux_dens	Incoming shortwave radiation	D	DI	DI	DI
downward_longwave_flux_dens	Incoming longwave radiation	D	DI	DI	DI
Ta	Air temperature	D	DI	DI	DI
pressure	Air pressure	D	DI	DI	DI
CO2_concentration	CO2 concentration at top of domain	D	DI	DI	DI

5.3 Driving Data

ACASA requires 8 input variables for each timestep of the model describing the meteorology and input radiation of the site (Table 1). These data must be continuous (i.e. free of gaps). At Tonzi, the site experienced a prolonged power outage during the summer of 2012 resulting in extended gaps of some input data. Therefore, we used input data from the Carbon Dioxide Information Analysis Center at Oak Ridge National Laboratory (http://cdiac.ornl.gov), which provides a core set of continuous meteorological data built off of data collected at various Ameriflux sites. CDIAC provided all the necessary continuous data for 2012 for Tonzi except for CO_2 concentration. Continuous CO_2 input data was generated by de-spiking and gap-filling CO_2 data collected at the site

At Wind River, there were no extended data gaps. CO_2 and wind speed were de-spiked to provide smooth input data to the model. Water vapor, CO_2, wind speed, incoming longwave radiation, air temperature, and air pressure were all gap-filled; however, none had more than 3% of the data missing.

At Diablo, data availability was high for most input data. CO_2 concentration, specific humidity, and pressure were missing 8% of the data. Additionally, spike algorithms were used to eliminate outliers in the CO_2 data resulting in gap-filling of 10% of the data during this period. Wind speed had 7% of the data missing. During the period from November 2012 – May 2013, and after applying the spike filter, 3% of [CO_2] data required gap-filling. Absolute humidity, wind speed and pressure required 1% or less of the data to be gap-filled whereas the remaining inputs were complete.

Gaps shorter than 3 hours were gap-filled using a simple linear regression at all sites. Gaps longer than 3 hours were filled using the mean diurnal trend of a 10-day or 20-day window centered on the day of the gap.

5.4 Modeling Approach

The ACASA model has been modified over the years to simulate fluxes at a variety of ecosystems including an evergreen needleleaf forest (e.g., Pyles et al. 2004), irrigated orchard (Falk et al. 2014), and Mediterranean shrubland (Marras et al. 2011). Most of the model validation has been done, however, for the Wind River needleaf forest. The site is evergreen and therefore seasonality in carbon uptake is driven by meteorology rather than significant changes in leaf area index (e.g., Wharton et al. 2012). Furthermore, the roots are within 2 meters of the surface, simplifying simulations of soil moisture and temperature. In order to run ACASA at a wide range of sites with stronger seasonality and water limitations, we developed and tested different modifications to ACASA resulting in four versions of the model (V1-V4) (Table 2).

As discussed above, ACASA parameters include initial soil temperature and moisture. Because low water availability is a strong environmental driver of fluxes in the Western U.S.—and at the sites that we chose to model—we were interested in how the ability of the model to simulate the belowground environment would impact the simulation of aboveground fluxes. We tested the model sensitivity to soil moisture and soil temperature by running both continuous and reinitialized simulations across the period of interest at all sites.

In the first approach (referred to as V1), we modeled fluxes without any major changes in the parameterization or initialization. Green leaf area index and photosynthetic capacity are determined in the parameterization file and remain constant throughout the time period of interest. After initialization, soil moisture and soil temperature are continuously modeled by ACASA throughout the period of interest.

In the second approach (V2), we incorporated green LAI seasonality into the dynamics of ACASA. LAI is no longer a constant parameter but rather part of the data driving the model. This is an important first step for using ACASA at non-evergreen sites and on timescales that overlap with changing phenology.

The third approach (V3) specifically addresses the ability of ACASA to model soil moisture and soil temperature over extended time periods as well as seasonal changes in green LAI. In V3, we re-initialized soil moisture, soil temperature and green LAI two times per month based on measurement data. We did this in order to constrain the modeled soil moisture and temperature from deviating strongly from the measurements. This should be especially important at sites that have very complex belowground hydrology or have roots that extend beyond the region modeled with ACASA.

Finally, in V4 we re-initialized soil temperature, soil moisture and green LAI as in V3 and additionally re-initialed photosynthetic capacity on a bi-monthly time step. Seasonality of photosynthetic capacity is especially important at sites with strong environmental limitations on photosynthesis that do not result in changes in LAI. Under environmental limitations, carbon fluxes may change based purely on biophysical stress response. Therefore, constraining the model with time-resolved values of photosynthetic capacity allowed us to assess ACASA's ability to simulate biospheric response to environmental drivers under stress. V4 should be especially important for modeling the processes at Tonzi under summer drought stress.

Table 2: Modifications made to ACASA resulting in versions V1-4.

	continuous or restart mode	**soil moisture/ soil temperature**	**green leaf area index**	**photosynthetic capacity**
V1	continuous	initialized on day 1 of simulation	constant	constant
V2	continuous	initialized on day 1 of simulation	driving variable (daily time step)	constant
V3	restart	reinitialized on day 1 and 15 of each month	reinitialized on day 1 and 15 of each month	constant
V4	restart	reinitialized on day 1 and 15 of each month	reinitialized on day 1 and 15 of each month	reinitialized on day 1 and 15 of each month

Chapter 6: ACASA as a Gap-Filling Tool

6.1 Simulation Periods

At Tonzi, we focused on the period of foliation of the blue oaks, modeling from March 1-October 31 in 2012. At Diablo, we modeled the period from November 2012 – May 2013, which coincides with the first precipitation events and the greening of the canopy and ends when the grasses have senesced. At Wind River, we modeled the evergreen conifer canopy for all of 2010.

6.2 Results

6.2.1 Soil Moisture

During 2010, Wind River received just over 3.5 m of precipitation. The measurements in Figure 21 show a clear response of soil moisture to precipitation events both at 20 cm and 50 cm. In the model, however, soil moisture tends to be unstable around precipitation events, quickly reaching field capacity (as noted by the upper threshold in modeled soil moisture), and then dries more rapidly than the measurements indicate. Two small precipitation events in the dry summer at Wind River demonstrate that ACASA overestimates the impact that a small precipitation event has on the soil, again both at 20 cm and 50 cm. After each rain event, soil moisture spiked at both depths whereas the measurements show that the soil remained dry despite these events; the ground is largely buffered by the forest's high LAI. Very little difference is noticeable at either depth between the continuous and the reinitialized versions of ACASA (V1 versus V3). The difference is most notable at the surface toward the end of the 2010 when V1 simulated a much drier soil despite the precipitation events.

During the period of the simulation in 2012, Tonzi received 325 mm of precipitation with just over 5 mm during the summer. This provided ideal conditions to assess both the simulated soil response to precipitation as well as the simulated dry-down through the summer. During the spring, the four versions of ACASA were not distinguishable from each other. Due to the resolution of ACASA belowground, Figure 21 shows the soil moisture measurements at 20 cm and simulation at 50 cm. As such, it is to be expected that measurements indicate higher soil moisture than ACASA. However, the response to precipitation should be more muted at the 50 cm simulation depth than the 20 cm measurement depth. To the contrary, the simulations show a much more rapid dry-down after each precipitation event. During the summer dry-down, ACASA overestimates both the rate of dry-down as well as the minimum soil moisture at the site. This is consistent at both depths shown. At Tonzi, the difference between the continuous runs (V1 and V2) and the re-initialized runs (V3 and V4) becomes apparent during the summer dry down. While all four runs predict a spike in soil moisture in response to a small precipitation event around DOY 150-2012, V3 and V4 are reinitialized to reflect the average state of the soil column, thus inducing more rapid dry-down than in V1 and V2. Overall, ACASA simulated a soil column that was overly sensitive to precipitation events and much drier during the summer than measurements indicate. Reinitializing soil moisture and temperature resulted in ACASA runs that actually deviated further from the measurements.

The Diablo site received 196 mm of precipitation from November 2012 – May 2013 with no precipitation after 07 April 2013 (DOY 97-2013). In all versions of ACASA (V1 – V3 at Diablo), the model over-estimated the threshold for soil moisture. Similar to the other sites, the ACASA simulated soil column

was overly sensitive to precipitation events with each event producing a strong spike both at the surface and at 50 cm. The measurements indicate that spikes did occur at both depths but they occurred to a lesser extent. In contrast to Wind River and Tonzi, ACASA underestimated the speed with which the soil dried after a precipitation event at Diablo. Additionally, ACASA overestimated the minimum threshold of soil moisture by nearly 20%, with soil drying to 0.23 $m^3 m^{-3}$ in V1 and V2 whereas the measurements indicated a minimum soil moisture of 0.04 m^3 m^{-3} at the end of the simulation period. Re-initializing soil moisture in V3 reduced the soil moisture closer to measurements; however, this effect was undone during a precipitation event. As such, soil moisture in V3 showed distinct discontinuities at each reinitialization.

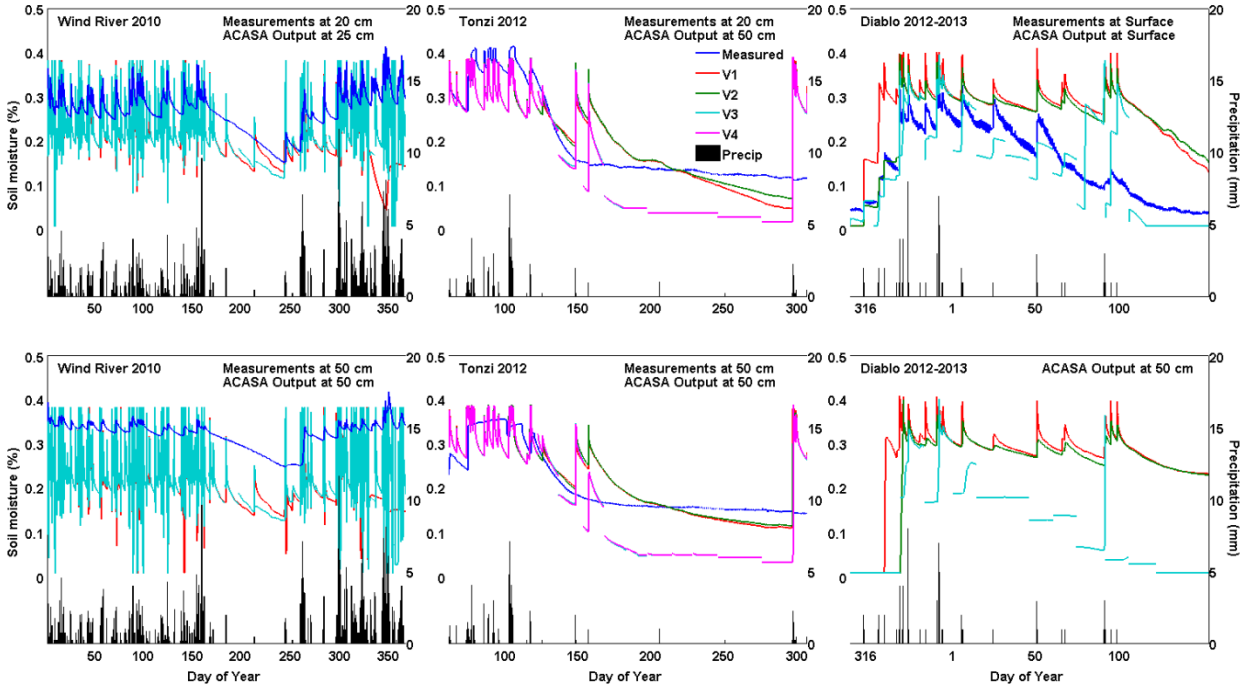

Figure 21: Soil moisture and precipitation for each version of ACASA at Wind River (left), Tonzi (middle), and Diablo (right) at two depths each.

6.2.2 Soil Temperature

At Wind River, surface temperatures from V1 and V3 were nearly indistinguishable (Figure 22). Both showed higher maximum temperatures and lower minimum temperatures than the measurements. This effect was greatest in the summer. Around DOY 200 (mid-July), for example, ACASA estimated a daytime maximum temperature of ~30ºC and a nighttime low surface soil temperature of less than 5ºC. Soil temperature measurements at the surface, however, showed temperatures ranging only from ~14ºC to 16.5ºC across a 24-hour period. In the simulation, the diurnal temperature range was much lower at 25 cm, although it was still greater than the measurements. Both V1 and V3 overestimated 30 cm soil temperatures with V3 being higher than V1. Model-measurement agreement was highest during the beginning of 2010. During the summer, V3 overestimated soil temperature at 25cm to a greater extent than V1. As the actual 30 cm soil temperature decreased in autumn, ACASA overestimated the cooling. However, the timing of the cooling and the direction of the change in temperature agreed with the measurements. Overall, ACASA simulated the 30 cm temperatures more accurately than the surface temperatures. Wind River simulations were not largely affected by re-initializing the model bi-monthly.

At Tonzi, the simulated diurnal range of soil surface temperature was the largest with a mid-summer range from 11.5ºC to 37ºC in a single day whereas the measurements indicated a range from 20.5ºC to 27ºC on the same day. The maximum soil surface temperature simulated by ACASA was 47.0ºC, 15ºC higher than the maximum measured. Re-initializing the model bi-monthly did not largely affect the results at the surface. At 30 cm, however, V3 and V4 simulated consistently higher temperatures, both at day and night, than V1 and V2 and the measurements. Most notable, however, ACASA tended to overestimate the diurnal trend in temperature at Tonzi.

The surface soil temperature simulations at Diablo also indicated a much higher diurnal range of temperature than the measurements indicated. The general seasonal trend, however, agreed with measurements in all 3 versions. From V1 to V3, the diurnal range in temperature increased. At 25 cm, the diurnal range in temperature was reduced from the surface but still much larger than the measurements indicated. The effect of variable vegetation in V2 reduced simulated soil temperature from V1. The trend throughout the simulation period generally agreed with the measurements.

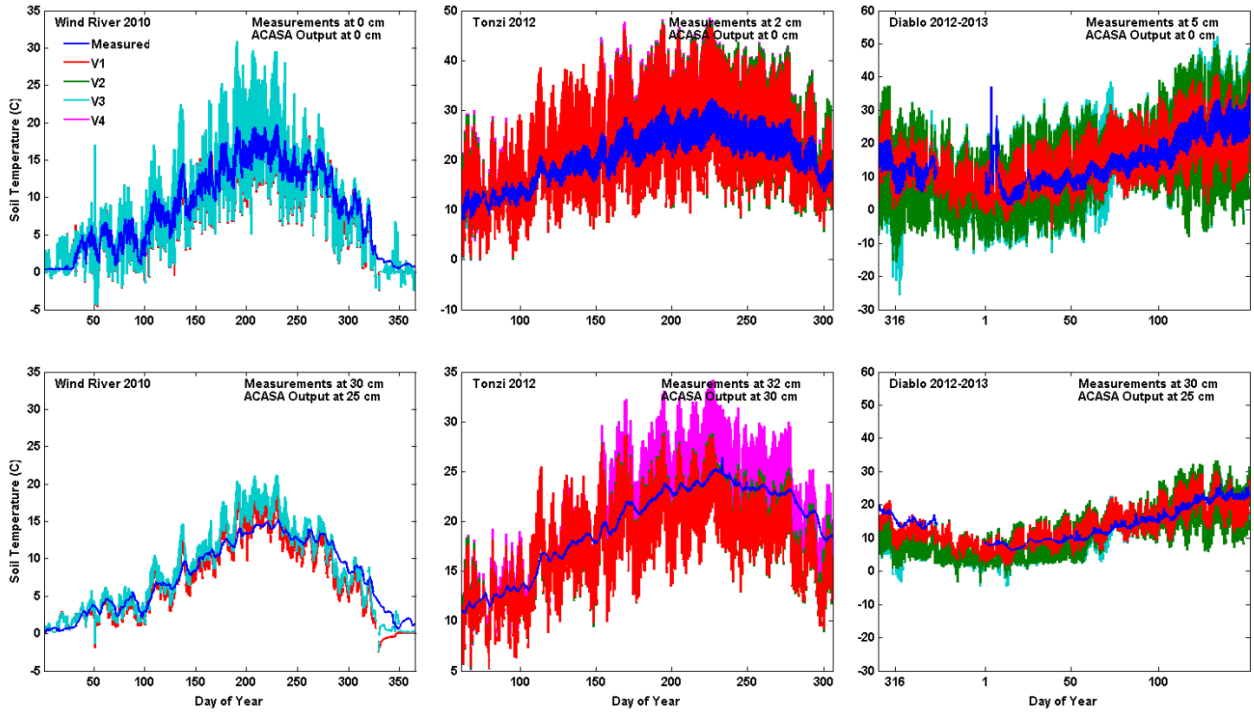

Figure 22: Soil temperature at Wind River (left), Tonzi (middle), and Diablo (right) at two depths and for all ACASA versions.

6.2.3 Net Ecosystem Exchange

NEE responds to environmental drivers such as temperature, incoming photosynthetically active radiation (PAR), and water availability. In the original ACASA model, NEE did not respond to changes in temperature or water level, showing a constant diurnal trend of photosynthesis regardless of strong seasonal trends in environmental drivers at the Tonzi AmeriFlux site. After collaborative work on the model led by the developers at UC-Davis, both the structure of the code as well as the dynamics improved, producing diurnal trends of NEE that responded to environmental drivers.

In order to assess ACASA performance in simulating NEE, we compared the average diurnal trend for each month of a simulation to the measurements. Figure 23 shows ACASA results for all versions of the simulations at all sites. In general, ACASA responded well to changes in environment drivers. Nighttime ecosystem respiration was in good agreement between the simulations and the measurements at both Wind River and Tonzi.

At Wind River, V1—the continuous simulation—agreed with measurements more than V3. While V1 and V3 slightly overestimated uptake during the winter months of January, February, November, and December, V1 accurately estimated uptake during the remainder of the year. During the summer drought, photosynthetic uptake tends to be suppressed during the midday (Wharton et al. 2009b). V1 simulated this midday depression of photosynthesis during July and August, leading to peak uptake occurring earlier in the day as well. The measurements from this period indicate a peak at 1200 or 1300 PST. V3, however, produced simulations that had stronger uptake in the summer, with the peak uptake remaining at nearly -15 µmol m^{-2} s^{-1} despite actual measurements indicating a peak of around -6 µmol m^{-2} s^{-1} during June and July.

Tonzi has a canopy of deciduous oaks with short-lived annual grasses on the ground. Here, we ran ACASA in all 4 configurations at this site. V1 and V2—the continuous simulations—simulated peak values of NEE uptake throughout the year that agreed well with measurements. However, similarly to Wind River, ACASA simulated a strong midday depression in V1 and V2 that results in net ecosystem respiration occurring by mid-afternoon from June – September. Throughout most of the simulation, V1 and V2 simulations were not significantly different. In April and May, however, V2 estimated stronger uptake than both V1 and the measurements. Re-initializing soil moisture, soil temperature, leaf area index (V3), and V_{cmax} (V4) resulted in the biggest difference in estimates from the continuous simulations during April, May, and June. As shown in Table 3 the reinitialized simulations (V3 and V4) overestimated maximum uptake (minimum NEE) in the months of April through June. Through the remainder of the year, the main difference between the continuous and the reinitialized simulations was that the reinitialized simulations predicted net uptake throughout most of the day, whereas in the continuous simulations the midday depression of uptake resulted in net ecosystem respiration.

The simulation period for Diablo occurred during multiple phenological stages of the grass canopy. At the beginning of the simulation, no green grass was visible and green LAI was 0. As such, the continuous ACASA simulation overestimated midday uptake. By December, there was a small amount of green grass and the reinitialized ACASA simulations estimated net near-neutral NEE. The measurements showed that despite the dominance of the previous year's senesced canopy, the emerging grass underneath was significantly productive, resulting in NEE of -4 µmol $m^{-2}s^{-1}$. While changes in measureable LAI were integrated into the bi-monthly reinitialization of ACASA simulations, this version of ACASA resulted in a vastly underestimated NEE. The continuous simulations with a constant LAI (V1) most closely captured the trend of NEE across the simulation period. The trend of NEE over the period was muted compared to measurements with V1 overestimating NEE during the November, December and April and underestimating peak fluxes during February and March. Variable LAI and reinitalizations for soil temperature, soil moisture and LAI resulted in suppressed fluxes throughout the majority of the simulation period. V2 and V3 predicted net uptake of CO_2 in March and April only.

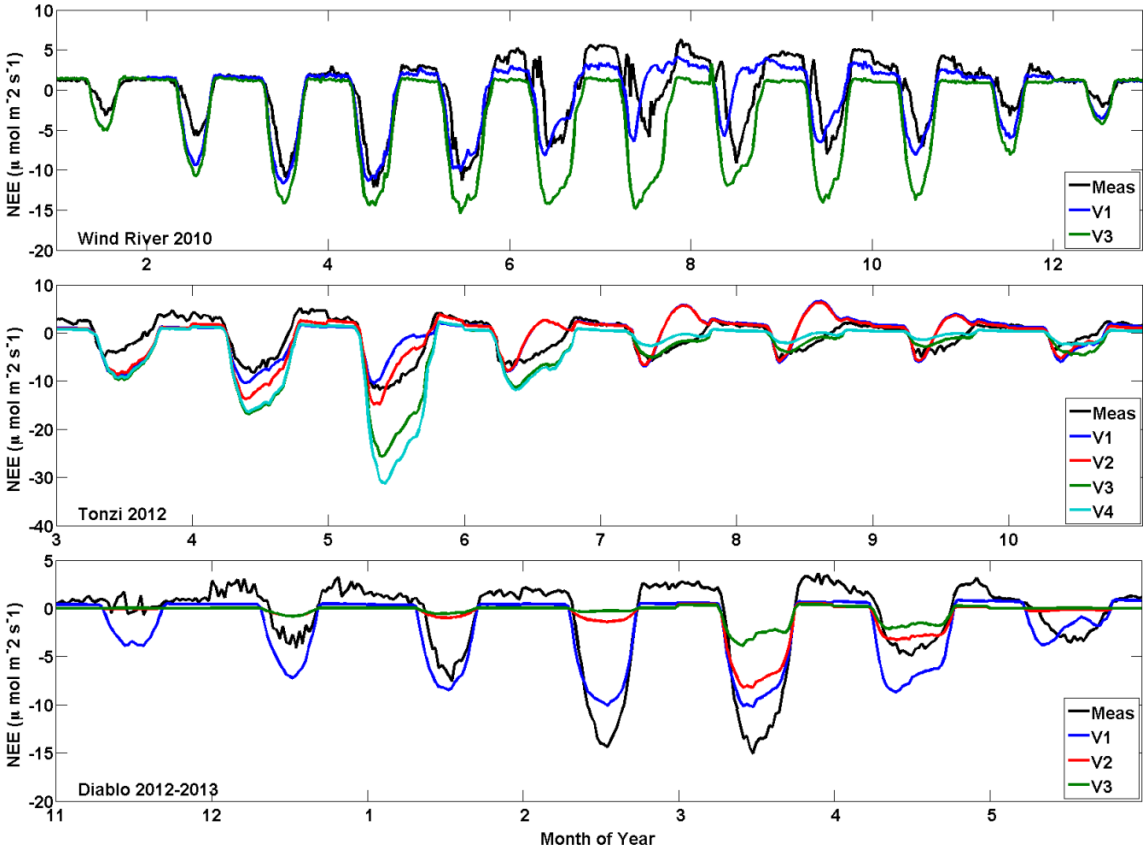

Figure 23: Mean monthly diurnal net ecosystem exchange (NEE) at Wind River in 2010 (top), Tonzi in 2012 (middle), and Diablo from 2012-2013 (bottom) for all versions of ACASA. Negative fluxes indicate net carbon uptake; positive fluxes indicate net carbon emissions.

Table 3: Mean minimum NEE (μmol $m^{-2}s^{-1}$) and mean maximum latent heat exchange (Wm^{-2}) for peak months at each site and for each simulation. Positive fluxes indicate an upward transport of heat.

	Minimum NEE (μmol m^{-2} s^{-1})					Maximum Latent Heat (W m^{-2})				
Simulation Month	**Meas.**	**V1**	**V2**	**V3**	**V4**	**Meas.**	**V1**	**V2**	**V3**	**V4**
Wind River										
April	-12.1	-11.3		-14.4		84.6	82.7		92.4	
May	-11.3	-10.3		-15.4		78.9	105.9		124.8	
June	-7.1	-8.2		-14.3		82.6	111.3		140.5	
Tonzi										
April	-8.2	-10.4	-13.8	-16.9	-16.4	212.3	132.0	148.3	180.6	177.0
May	-11.8	-10.5	-14.9	-25.7	-31.3	248.6	112.5	140.0	226.7	273.6
June	-7.4	-8.0	-7.9	-11.4	-11.9	113.4	116.3	115.0	157.0	165.0
Diablo										
January	-7.6	-8.5	-1.0	-0.6		78.5	65.5	18.8	16.2	
February	-14.4	-10.1	-1.4	-0.3		140.9	91.5	29.0	23.2	
March	-15.0	-10.2	-8.2	-3.8		145.4	120.6	101.7	66.0	
April	-4.9	-8.7	-3.3	-2.1		82.2	65.5	18.8	16.2	

6.2.4 Latent Energy Exchange

Simulated latent energy (LE) at Wind River agreed well with measurements (Figure 24). At Wind River, the continuous simulation (V1) performed the best, with only slight overestimation of LE during the peak months from May through August (Table 3). V3 predicted LE in good agreement with the measurements during the winter. However, during the period from May through September, V3 estimated much higher LE fluxes than both the measurements and V1. By the end of the simulation period in November and December, the V3 LE fluxes agreed well with the measurements and with V1.

In the first month of simulation at Tonzi, LE from all versions of ACASA agreed well with measurements. In the spring, the reinitialization resulted in V3 and V4 closely simulating peak LE fluxes during April and May. The continuous versions of ACASA underestimated LE compared to measurements. Throughout the summer, there was very little difference between the versions of ACASA and all versions overestimated LE. The measurements showed that actual LE decreased from 67 W m^{-2} in July to only 23 W m^{-2} in September. The mean of all 4 versions of ACASA estimated LE from 127 W m^{-2} in July to 98 W m^{-2} in September.

At Diablo, measurements indicated that latent heat exchange varied from between 50 W m^{-2} to 150 W m^{-2} throughout the simulation period. In general, V2 and V3—with variable LAI—underestimated LE. Simulated LE from V1 remained around 50 W m^{-2} from November through January, and around 100 W m^{-2} from March through May. V2 and V3, however, estimated LE fluxes of only 18-30 W m^{-2} from November through February. The seasonal trend in LAI resulted in model-measurement agreement between with V2 and V3 only in April.

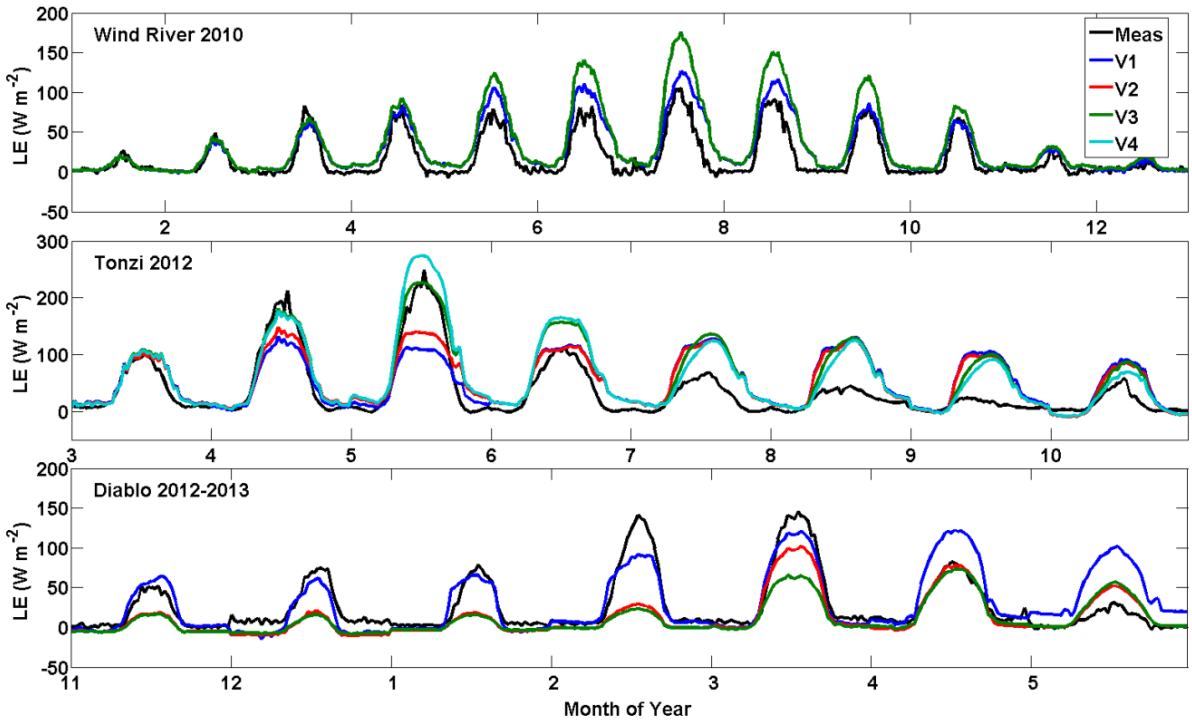

Figure 24: Seasonal trends of latent energy (LE) flux throughout the simulation period at Wind River (top), Tonzi (middle), and Diablo (bottom) for versions 1 - 4 of ACASA.

6.2.5 Sensible Energy Exchange

The sensible heat flux at Wind River did not vary significantly between V1 and V3 (Figure 25). ACASA generally was able to simulate the seasonal trend of H at the site; H fluxes were low in January, increased to a peak in July, and then decreased throughout the remainder of the year. However, the magnitude of H was strongly overestimated. Measurements indicated that the maximum H was 347 W m^{-2} in July whereas ACASA simulated H of 597 W m^{-2} in the same month. During the winter months of January, November, and December the measurements indicated no diurnal trend in H. ACASA however, predicted a positive H of up to 133 W m^{-2} during the same months.

Similar to Wind River, the simulated H flux at Tonzi was higher than the measurements, but matched the general trend with a peak in July. V2 predicted H fluxes were slightly higher than the other versions from April through May. All daytime peaks were greater than the measurements with the observations indicating the highest H in July of 405 W m^{-2} whereas ACASA predicted 645 W m^{-2} in the same month.

At the Diablo site, simulated H agreed more with the measurements than at the other sites. The biggest discrepancy occurred during February and March when ACASA overestimated H by 188 and 162 W m^{-2}, respectively. Aside from February and March when H was overestimated, V2 had the best agreement with the measurements.

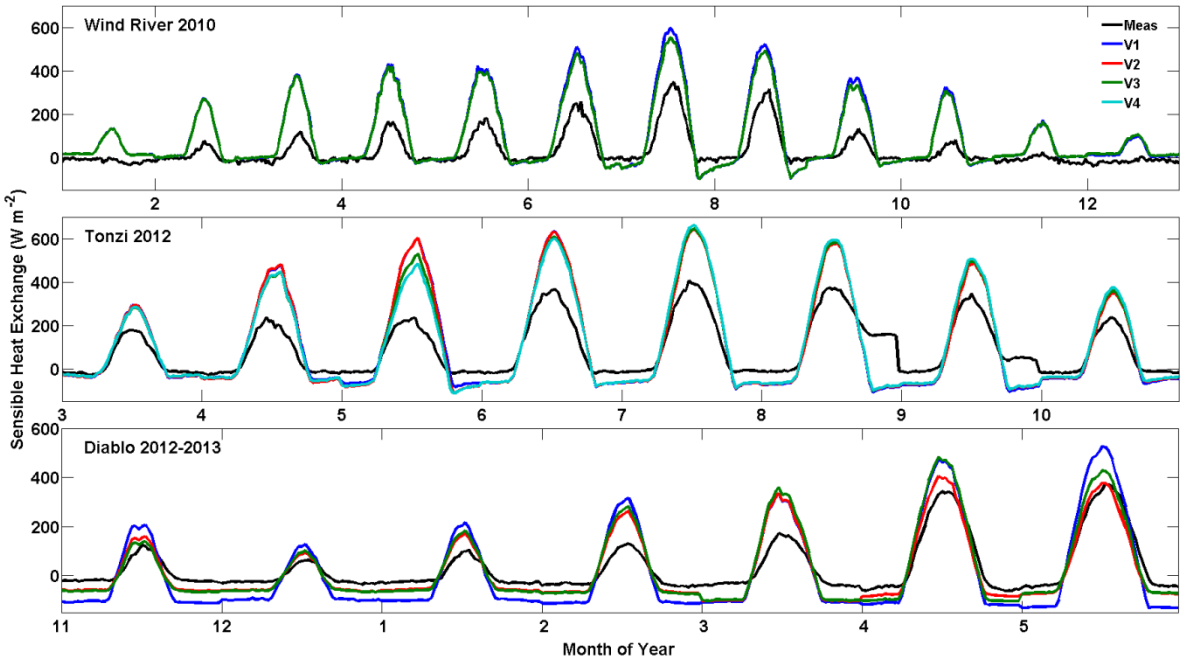

Figure 25: Mean monthly diurnal trend of sensible heat (H) flux at Wind River (top), Tonzi (middle), and Diablo (bottom) for each of the ACASA versions 1 - 4.

6.3 Discussion

6.3.1 Impact of Soil Reinitialization

In the ecosystems that we modeled, water is a strong limitation to NEE due to the Mediterranean climate, even at Wind River which usually receives over 2 m of precipitation a year. At Tonzi and Diablo, the soil

is rarely saturated and the soil dry-down dynamics are important for determining the extent of water limitation on NEE. In ACASA, dry soils result in a decrease in photosynthetic capacity depending on the soil type and the soil moisture. In V1 of ACASA, soil moisture is simulated continuously and any error in modeling may be compounded through time. However, we did not see an improvement in simulating NEE at any site with V3 where soil moisture was reinitialized based on measurements twice monthly. ACASA simulates soil conditions for the number of layers determined in the parameterization of the model. Often, this results in a modeled soil profile much deeper than the profile of soil represented in measurements. Additionally, initial soil conditions are given only as a single value and then propagated to create a soil profile in the 2nd timestep. We calculated initial soil conditions based on the average of the values for the profiled measurement. The reinitialization of soil moisture had a larger impact during dry periods than during wet. At Wind River where soil moisture was high throughout much of the year, there was very little difference between simulations of soil moisture by V1 and V3.

During the simulation periods at Diablo and Tonzi, both sites experienced a wider range of soil moisture, with long periods when the soil was very dry. Simulations during this period suggest that ACASA performs better in wet soils than in dry. At both sites, a precipitation event occurred late in the simulation period after the soil had dried completely. During the dry period, V1 and V2 of ACASA predicted higher soil moisture than measurements indicated. However, after the precipitation event, all versions increased soil moisture to similar values. The accuracy of ACASA soil moisture, however, is not consistent across sites. Because the soil at Tonzi and Diablo was often dry, the complexities of the soil profile had a larger effect on the ability of ACASA to simulate soil moisture and temperature. For example, minimum soil moisture at a site is used as a parameter. However, a single value is not representative of the entire soil column. Thus, the accuracy of ACASA-simulated soil conditions varied throughout the column depending on stage of dry-down.

Overall, reinitializing soil moisture and soil temperature did not improve model estimates of the soil conditions at any site. Current work is being done at UC-Davis to improve the performance of the soil module in ACASA. This work should focus on simulating the soil response to precipitation as well as dry-down dynamics. Additionally, improvements could be made in translating single values of soil characteristics in the parameterization file to dynamic profiles representative of a complex soil column.

6.3.2 Impact of All ACASA Modifications on Flux Exchange

In this study, we were specifically interested in the ability of ACASA to simulate net ecosystem exchange for a range of ecosystems. ACASA has been extensively tested for Wind River, a site that does not have strong gradients in LAI or photosynthetic capacity throughout the year. However, at sites with a non-evergreen canopy (i.e. deciduous trees, perennial or annual grasses etc.), changes in LAI can occur rapidly and thus should be taken into consideration when modeling the fluxes. Additionally, previous research from Tonzi shows that photosynthetic capacity can vary greatly throughout the season. As such, we aimed to constrain the belowground portion of the model with the reinitialization and then test the sensitivity of the aboveground portion to finely-tuned parameterizations in V2 and V3 of ACASA.

At Wind River, the soil is buffered from rapid changes in moisture and temperature due to a large dense canopy above. As such, we predicted that finely-tuning and constraining the belowground microenvironment would not have as big of an impact on LE and NEE as it would at sites like Tonzi and Diablo where large portions of the ground are exposed or where the water table depth is deeper. We did,

however, observe large differences in predicted NEE and LE between V1 and V3 with V1 agreeing best with the measurements. Because LAI is largely constant throughout the year at Wind River, the only changes between V1 and V3 at the site were updated soil moisture and temperature. As discussed above, ACASA tends to more accurately simulate the soil microenvironment when moisture is high. Thus, attempting to constrain the soil module during the wet year at Wind River instead caused disruptions the model-simulated soil profile.

At Tonzi, V3 and V4 also overestimated NEE and LE during the spring peak months despite the LAI, soil moisture and temperature, and photosynthetic capacity being representative of actual values at the site during that time. This is due to the fact that ACASA is a single column model and therefore does not assimilate any spatial heterogeneity into the model but rather assumes a consistent cover from the canopy information. A savannah, however, is a patchy system with some areas covered only with grass and other areas with both grass and trees. The peak LAI during April and May represented the sum of LAI from both the grasses and trees. By incorporating maximum LAI into ACASA, fluxes of both NEE and LE were overestimated because ACASA calculates fluxes based on a constant LAI across the site. Additionally, ACASA assumes that photosynthetic capacity is constant throughout the canopy. At Tonzi, the photosynthetic capacity of the blue oaks is much higher than most deciduous broadleaved trees and also much higher than the grasses (Xu and Baldocchi 2003). Therefore, by parameterizing ACASA with high photosynthetic capacity during the period with the highest LAI (accounting for the live grasses), ACASA-estimated NEE is well above the measurements. As the summer drought initiates, LAI decreases as the grasses die and some trees begin to lose leaves. While ACASA can assimilate the changes in LAI, the distribution of LAI throughout the canopy remains constant in the model. ACASA assumes an active grass layer throughout the entire summer instead of a single-layer canopy with only active trees. Additionally, uptake is reduced in all versions due to the drought effect on photosynthetic capacity incorporated automatically in response to the soil moisture, and through reinitialization in V4.

The Diablo AmeriFlux site was included to represent ecosystems on the opposite end of the spectrum from Wind River in terms of LAI seasonality, canopy complexity, and canopy height. Our work indicates that interactions between aboveground and belowground microclimates were important at Diablo. During December and into January when soil moisture was high, V1 agreed with the measurements whereas V2 and V3 were unable to capture the actual NEE during this time period, predicting near-neutral carbon fluxes. An additional factor contributing to the model-measurement agreement is that the grasses were parameterized with sparsely available literature values typical of similar grasslands. Photosynthetic capacity varies largely as nitrogen availability in the soil varies and thus parameterizing a grassland is difficult without measurements of either photosynthetic capacity or leaf nitrogen content from the site. With a short grass canopy that has roots concentrated in the upper layers of the soil, our study indicates that both aboveground and belowground microclimates in the upper soil layer have a strong impact on accurately simulating both NEE and LE.

Overall, ACASA performed well in simulating fluxes of NEE, LE, and H. Contrary to our expectations, we did not see a systematic improvement in model performance after incorporating high temporal resolution LAI, photosynthetic capacity, or soil property information. V2-V4 performance was not significantly better than V1, and in many cases performance was poorer.

Chapter 7: Conclusions

Gaps exist in our current understanding of CO_2 flux exchange which leads to errors in biospheric sink/source estimates. For example, the research community currently doesn't fully understand mechanisms for eddy covariance CO_2 flux outliers may be atmospheric-driven. This is especially true at night when turbulence is intermittent and produced by shear often above the canopy. Furthermore, our methods for gap-filling missing or erroneous CO_2 flux data are inadequate, especially, when long data records are missing at the more ecologically complex flux sites.

Here, we approached reducing the uncertainty in biospheric CO_2 flux in two ways. First, by introducing vertically-profiling lidar at flux towers to measure atmospheric processes well above the height of typical eddy covariance instruments. At open canopies, lidar also allows for measurements of flow within the subcanopy. And second, by modifying and testing a 3rd order closure, land surface model for more accurate simulations of fluxes. The ACASA model was validated here for a wide range of flux tower sites along the West Coast, USA.

During our field campaigns we measured evidence of along-axis mountain-valley flow reversals, cross-axis katabatic/anabatic slope flows, nocturnal drainage flows, and "top-down" forced turbulence events. Of these phenomena, intermittent "top-down" forced turbulence had the strongest impact on eddy covariance ecosystem fluxes. This was evident at Tonzi as the open oak-savannah allowed for lidar deployment within the canopy. Turbulence from these events was able to penetrate the canopy and provided a mechanism for transporting understory CO_2 emissions to the height of the eddy covariance instrumentation. On nights without these strong turbulence bursts, such as during katabatic flow events, turbulence did not penetrate as deep into the canopy and the EC instruments systematically underestimated the ecosystem CO_2 exchange. Deploying a lidar at other suitable sites would provide more definitive answers for how important above-canopy, atmospheric-driven turbulence is for causing EC CO_2 flux anomalies and errors.

We showed that the ACASA model has the ability to accurately simulate fluxes of carbon dioxide, water and energy across the extreme range of ecological, climatic, and hydrological gradients found on the American West Coast. The next step is to quantify the errors in the annual carbon sink/source budgets which result from using ACASA as a gap-filling tool to replace missing or erroneous fluxes in the eddy covariance data record. We expect that these errors will be reduced significantly at multi-layered forest canopies in comparison to simpler modeling approaches, such as those done with a "big-leaf" model. However, a 3rd order closure model such as ACASA may not be needed for single layer canopies, such as grasslands, which may require instead a more sophisticated treatment of belowground processes. Further work is warranted in this area.

Significant deliverables from our 3-year project included (1) the development of a new research site at Site 300 for boundary layer-CO_2 research, including the addition of an unmanaged grassland tower to the AmeriFlux network called Diablo, (2) the novel use of atmospheric lidar for interpreting eddy covariance flux errors and anomalies at flux tower sites, and (3) the modification of ACASA for simulating biospheric CO_2 fluxes at a wider range of ecosystems and climates.

Our project strengthened cross-collaborations between atmospheric and terrestrial carbon researchers at LLNL and provided a springboard for future collaborative work between CAMS, NARAC, and PCMDI,

including new capabilities for land surface modeling with ACASA and a test site for terrestrial carbon research/boundary layer at Site 300. These cross-collaborations led to ideas put forth in two funded LDRD proposals: "Tracking Water through the Critical Zone to Assess Drought Vulnerability, 15-ERD-042" and "Unveiling a Mini-TDL to Measure Partitioned CO_2 Fluxes, 14-LW-079".

This project also strengthened LLNL's collaborations with universities and national laboratories including the University of California, Davis, University of California, Berkeley, University of Oklahoma, University of Washington, Seattle, San Diego State University, Oregon State University, Lawrence Berkeley National Laboratory, and Pacific Northwest National Laboratory through either direct collaboration or through invited talks. Furthermore, our capabilities in land surface-atmosphere dynamics were shown to the DOE Office of Science's Biological and Environmental Research (BER) Program through presentations and invited talks at the North American Carbon Program Annual Meeting and the AmeriFlux Annual Meeting.

Of final note, WRF-ACASA (described in brief in Chapter 5.1) has recently been incorporated into the Massachusetts Institute of Technology's (MIT) Integrated System Model (IGSM) framework by our colleagues at MIT. Future collaborations with these colleagues would highlight and leverage LLNL's strengths in mesoscale and climate modeling. Fine tuning land surface processes in mesoscale (WRF-ACASA) and climate (IGSM-CAM-WRF-ACASA) models is an area of high interest with the DOE Office of Science's BER program. Relevant programs that would benefit from such research include the Atmospheric Radiation Measurement (ARM) Climate Research Facility and the Next-Generation Ecosystems Experiments (NGEE).

Chapter 8: List of Presentations, Manuscripts, and Author Contributions

8.1 List of 12-ER-043 Presentations (19 total)

8.1.1 Professional Conferences

1. Falk, M., Wharton, S., Pyles, R.D., and J. Osuna, 2012. Reducing Uncertainty in Biospheric CO_2 flux, *Proceedings 30th Conference on Agricultural and Forest Meteorology*, 28 May 28-1 June 1 2012, Boston, MA, American Meteorological Society, Boston, MA

2. Falk, M., Wharton, S., Bible, K., 2014. Constraining Long Term Carbon Exchange over an Old-Growth Forest in Complex Terrain with ACASA. *Proceedings 31st Conference on Agricultural and Forest Meteorology*, 12-15 May 2014, Portland, OR, American Meteorological Society, Boston, MA, 4.3

3. Ma, S., Baldocchi, D., Vila-Guerau de Arellano, J., Osuna, J., Wharton, S., 2013. Surface Energy Balance: Lessons Learned from Modeling Simulations and Field Measurements at an Oak-Grass Savanna. *Eos Trans*. AGU, 94(52), Fall Meet. Suppl., December 2013

4. Osuna, J., Wharton, S., Falk, M., Ma, S., Paw U, K.T., Bible, K., Baldocchi, D., 2012. Preliminary Results of Modeling Turbulent Kinetic Energy at AmeriFlux Sites for Assessing Flux Quality. *Eos Trans*. AGU, 93(52), Fall Meet. Suppl., December 2012, LLNL-POST-607033

5. Osuna, J., R. D. Pyles, S. Ma, M .Falk, D. Baldocchi, S. Wharton., 2013. Modeling Fluxes at 2 Drought-Stressed Ecosystems with ACASA. *Eos Trans.* AGU, Fall Meet. Suppl. December 2013, LLNL-POST-647442

6. Osuna, J., R. D. Pyles, S. Ma, D. Baldocchi, K. Bible, S. Wharton, 2014. Using Canopy Models and Measurements for Improved Flux Interpretation. *Proceedings 31st Conference on* Agricultural and Forest Meteorology, 12-15 May 2014, Portland, OR, American Meteorological Society, Boston, MA, LLNL-POST-640675

7. Wharton, S., Osuna, J., Newman, J., Falk, M., Baldocchi, D., Bible, K., 2012. Atmospheric Lidar Provides Insight into Land Surface-Atmosphere Exchange at AmeriFlux Towers. *Eos Trans*. AGU, 93(52), Fall Meet. Suppl., December 2012, Abstract A13F-0266, LLNL-POST-605972

8. Wharton, S., Osuna, J., Falk, M., Newman, J., Ma, S., Baldocchi, D. Bible, K., 2014. Using Atmospheric Lidar to Interpret CO2 fluxes in Complex Terrain at Three AmeriFlux Towers. *Proceedings 31st Conference on Agricultural and Forest Meteorology*, 12-15 May 2014, Portland, OR, American Meteorological Society, Boston, MA, 4.4, LLNL-PRES-654614

8.1.2 LLNL Seminars and Reviews

9. Osuna, J., Wharton, S., and M. Falk, 2012. Using Field Measurements to Validate and Improve a Land Surface – Atmosphere Model of Trace Gas Exchange, LLNL Post-Doctorate Symposium, 17 July 2012, LLNL-POST-564456

10. Osuna, J., Wharton, S., Falk, M., 2012. Using Field Measurements to Validate and Improve a Land Surface – Atmosphere Model. Science and Technology Review, LLNL-POST-564456

11. Osuna J., S. Wharton, M. Bora, T. Bond, E. Garza, K. Bible, S. Ma, D. Baldocchi, R. D. Pyles, 2014. Improved Understanding of Ecosystem Flux Dynamics: An Integrated Approach through Modeling and Novel Measurements. LLNL Post-Doctorate Symposium, 9 July 2014, LLNL-POST-656819

8.1.3 Meetings with Potential Funding Sponsors

12. Osuna, J., Wharton, S., Falk, M., Ma, S., Baldocchi, D., 2013. A New Method for Reducing Uncertainty in Biospheric CO2 Flux: A Case Study at Tonzi AmeriFlux Site. 2013 TES/SBR Joint Investigators Meeting, Potomac, MD, 14-15 May 2013, LLNL-ABS-635392

13. Wharton, S., Osuna, J., Baskett, R., Hartmann, C., 2013. LLNL Hi-Resolution Evapotranspiration Modeling for Accurate Irrigation Management and Scheduling Tools. USDA/DOE Agricultural Technology Showcase, Fresno, CA, 13 Aug 2013, LLNL-PRES-615401

14. Wharton, S., Newman, J., Osuna, J., Ma, S., Falk, M., Bible, K., Baldocchi, D., 2013, Atmospheric Lidar Provides Insight into Land Surface-Atmosphere Exchange at 3 AmeriFlux Towers, 4th North American Carbon Program All-Investigators Meeting, Albuquerque, NM, 4-7 Feb 2013, LLNL-POST-605972

15. Osuna, J., Wharton, S., Falk, M., Ma, S., Baldocchi, D., 2014. A New Method for Reducing Uncertainty in Biospheric CO2 Flux: A Case Study at Tonzi AmeriFlux Site. 2013 AmeriFlux Principal Investigators Meeting, Potomac, MD, 4-5 May 2014, LLNL-POST-640675

8.1.4 Invited Talks

16. Osuna, J., Wharton, S. A New Method for Reducing Uncertainty in Biospheric CO_2 flux, Lawrence Berkeley National Laboratory, Berkeley, CA, 2012, LLNL-PRES-582996

17. Osuna, J., Wharton, S., Falk, M., Ma, S., Baldocchi, D., 2013. Toward an Improved Understanding of Flux Sources. 4th North American Carbon Program All-Investigators Meeting, Albuquerque, NM, 4-7 Feb 2013, LLNL-PRES-615592

18. Wharton, S. Long-Term Carbon Sink in an Old-Growth Forest: Lessons Learned from 15 Years of Flux Measurements at the Wind River Field Station, College of Forestry, Oregon State University, Corvallis, OR, 20 May 2013, LLNL-PRES-637433

19. Wharton, S. Lidar Applications for the Carbon Flux and Wind Energy Communities. School of Meteorology, University of Oklahoma, Norman, OK, 11 March 2013, LLNL-PRES-627420

8.2 Manuscripts in Preparation

Falk, M., Osuna, J., Pyles, R.D., Ma, S., Baldocchi, D., Bible, K., Wharton, S., Gap-filling data using a higher-order closure model at 3 AmeriFlux sites on the US West Coast. Planned submission to *Environmental Research Letters*

Osuna, J., Pyles, R.D., Falk, M., Ma, S., Baldocchi, D., Bible, K., Wharton, S. Evaluating the need for a higher-order closure model to simulate ecosystem fluxes at 3 contrasting AmeriFlux sites. Planned submission to *Agricultural and Forest Meteorology*

Wharton, S., Falk, M., Newman, J., Osuna, J., Ma, S., Baldocchi, D., Bible, K. Using wind lidar to identify atmospheric-induced flux anomalies at three distinct West Coast AmeriFlux towers. Planned submission to *Agricultural and Forest Meteorology*

8.3 Author Contributions

Sonia Wharton – Dr. Wharton was the Primary Investigator for the LDRD 12-ER-043 project. She and Dr. Falk wrote the proposal. Dr. Wharton was responsible for project management and the lead contributor for designing, conducting and analyzing the results of the canopy flows experiment (described in Chapter 4).

Dennis Baldocchi – Dr. Baldocchi is the Primary Investigator for the Tonzi AmeriFlux tower. He provided site access and intellectual contributions to the lidar and radiosonde experiments at Tonzi.

Ken Bible – Dr. Bible is the Site Director at the Wind River Field Station and Primary Investigator for the Wind River Ameriflux tower. Dr. Bible provided site access, invaluable knowledge of the forest ecology, and participated in the lidar and radiosonde experiments at Wind River.

Matthias Falk – Dr. Falk was a significant intellectual contributor to the project from start to end. He served as an ACASA mentor to Jessica Osuna. Dr. Falk also contributed his expertise in radiosonde and eddy covariance instrumentation during the design and execution of the lidar and radiosonde experiments.

Jessica Osuna – Dr. Osuna was the post-doctorate scholar on the project. Her primary role was to modify and execute the ACASA model for all sites. She also processed and analyzed the radiosonde measurements and participated in the lidar and radiosonde experiments.

Siyan Ma – Dr. Ma provided the above canopy and subcanopy Tonzi AmeriFlux eddy covariance data and invaluable knowledge about the site.

Jennifer Newman – Jennifer is a Ph.D. graduate student at the University of Oklahoma, Norman. Jennifer contributed her expertise in lidar theory and application. She also contributed to the data post-processing including the calculation of turbulence kinetic energy for the lidar data.

R. David Pyles – Dr. Pyles is a major intellectual contributor to the ACASA model and he contributed his modeling expertise to this project.

Matt Schroeder – Matt is the field technician at the Wind River AmeriFlux site. He provided invaluable help with site logistics, eddy covariance system maintenance and calibration, and lidar deployment at Wind River.

Chapter 9: References Cited

Acevedo, O.C., Moraes, O.L., Degrazia, G.A., Fitzjarrald, D.R., Manzi, A.O., Campos, J.G., 2009. Is friction velocity the most appropriate scale for correcting nocturnal carbon dioxide fluxes? *Agricultural and Forest Meteorology*, 149, 1-10

Arain, M., Black, T., Barr, A., Jarvis, P., Massheder, J., Verseghy, D., Nesic, Z., 2002. Effects of seasonal and interannual climate variability on net ecosystem productivity of boreal deciduous and conifer forests. *Canadian Journal of Forestry*, 32: 878-891

Baldocchi, D., 2008. "Breathing" of the terrestrial biosphere: lessons learned from a global network of carbon dioxide flux measurements. *Australian Journal of Botany*, 56:1-26

Baldocchi, D., Falge, E., Gu, L., Olson, R., Hollinger, D., Running. S., Anthoni, P., Bernhofer, C., Davis, K., Evans, R., Fuentes, J., Goldstein, A., Katul, G., Law, B., Lee, X., Malhi, Y., Meyers, T., Munger, W., Oechel, W., Paw U, K.T., Pilegaard, K., Schmid, H.P., Valentini, R., Verma, S., Vesala, T., Wilson, K., Wofsy, S., 2001. FLUXNET: A new tool to study the temporal and spatial variability of ecosystem-scale carbon dioxide, water vapor, and energy flux densities. *Bulletin of the American Meteorological Society*, 82(11): 2415-2434

Baldocchi, D., Xu, L., Kiang, N., 2004. How plant functional-type, weather, seasonal drought, and soil physical properties alter water and energy fluxes of an oak–grass savanna and an annual grassland. *Agricultural and Forest Meteorology*, 123, 13-39

Baldocchi, D., Tang, J., Xu, L., 2006. How switches and lags in biophysical regulators affect spatial-temporal variation of soil respiration in an oak-grass savannah. *J Geophysical Research*, 111, G02008, doi:10.1029/2005JG000063

Baldocchi, D., Ma, S., Rambal, S., Misson, L., Ourcival, J.-M., Limousin, J.-M., Pereira, J., Papale, D., 2010. On the differential advantages of evergreenness and deciduousness in Mediterranean oak woodlands: a flux perspective. *Ecological Applications*, 20, 1583-1597

Bonan, G.B., 1996. Land surface model (LSM version 1.0) for ecological, hydrological, and atmospheric studies: Technical description and users guide. NCAR Technical Note NCAR/TN-417+STR, doi:10.5065/D6DF6P5X

Cañadillas, B., Westerhellweg, A., Neumann, T., 2011. Testing the performance of ground-based wind LiDAR system. *DEWI Magazine*, 38, 58-64

Cariou, J.-P., Boquet, M., 2010. Leosphere pulsed lidar principles: contribution to UpWind WP6 on remote sensing devices. Available online at: http://www.upwind.eu/Publications/˜/media/UpWind/Documents/Publications/6%20%20Remote%20Sensing/D611.ashx

Chiesi, M., Maselli, F., Moriondo, M., Fibbi, L., Bindi, M., Running, S.W., 2007. Application of Biome-BGC to simulate Mediterranean forest processes. *Ecol. Modell*., 206, 179-190

Choi, W., Faloona, I., McKay, M., Goldstein, A., Baker, B., 2011. Estimating the atmospheric boundary layer height over sloped, forested terrain from surface spectral analysis during BEARPEX. *Atmospheric Chemistry and Physics*, 11, 6837-6853

Collatz, G.J., Ball, J.T., Grivet, C., Berry, J.A., 1991. Physiological and environmental regulation of stomatal conductance, photosynthesis, and transpiration: a model that includes a laminar boundary layer. *Agricultural and Forest Meteorology*, 54, 107-136

Dibley, V., Ferry, L, Buscheck, M. Anderson, A., Madrid, V., Chamberlain, P., McKereghan, P., Demir, Z., Radyk, J., Gregory, S., Taffet, M., Goodrich, R., Valett, J., Helmig, A., 2011. 2010 Annual Compliance Monitoring Report Lawrence Livermore National Laboratory Site 300. UCRL-AR-206319-10, 584 p.

Draxler, R.R., Hess, G.D., 1997. Description of the HYSPLIT_4 modeling system. NOAA Tech. Memo. ERL ARL-224, NOAA Air Resources Laboratory, Silver Springs, MD, 24 p

Draxler, R.R., Rolph, G.D., 2014. HYSPLIT (HYbrid Single-Particle Lagrangian Integrated Trajectory) Model access via NOAA ARL READY Website (http://ready.arl.noaa.gov/HYSPLIT.php). NOAA Air Resources Laboratory, Silver Spring, MD

Durden, D.J., Nappo, C.J., Leclerc, M.Y., Duarte, H.F., Zhang, G., Parker, M.J., Kurzeja, R.J., 2013. On the impact of wave-like disturbances on turbulent fluxes and turbulent statistics in nighttime conditions: a case study. *Biogeosciences*, 10, 8433-8443

El-Madany, T.S., Duarte, H.F., Durden, D.J., Paas, B., Deventer, M.J., Juang, J.-Y., Leclerc, M.Y., Klemm, O., 2014. Low-level jets and above-canopy drainage as causes of turbulent exchange in the nocturnal boundary layer. *Biogeosciences*, 11, 4507-4519

Falge, E., Baldocchi, D., Olson, R., Anthoni, P., Aubinet, M., Burba, G., Ceulemans, R., Clement, R., Dolman, H., Granier, A., Gross, P., Grunwald, T., Hollinger, D., Jenson, N., Katul, G., Keronen, P,, Kowalski, A., Lai, C.T., Law, B., Meyers, T., Moncrief, J., Moors, E.J., Munger, W., Pilegaard, K., Rannik, U., Rebmann, C., Sukyer, A., Tenhunen, J., Tu, K., Verma, S., Vesala, T., Wilson, K., Wofsy, S., 2001. Gap filling strategies for defensible annual sums of net ecosystem exchange. *Agricultural and Forest Meteorology*, 107: 43–69

Falk, M., Paw U, K.T., Wharton, S., Schroeder, M., 2005. Is soil respiration a major contributor to the carbon budget within a Pacific Northwest old-growth forest? *Agricultural and Forest Meteorology*, 135: 269-283

Falk, M., Wharton, S., Schroeder, M., Ustin, S.L., Paw U, K.T., 2008. Flux portioning in an old growth forest: seasonal and interannual dynamics. *Tree Physiology* 28, 509-520

Falk, M., Pyles, R.D., Paw U, K.T., Xu, L., Whiting, M.L., Sanden, B.L., Brown, P.H., 2014. Evaluated crop evapotranspiration over a region of irrigated orchards with the improved ACASA-WRF model. *J Hydrometeor*., 15, 744-758

Farquhar, G.D., von Caemmerer, S., Berry, J.A., 1980. A biochemical model of photosynthetic CO2 assimilation in leaves of C3 species. *Planta*, 149, 78-90

Fisher, J.B., Huntzinger, D.N., Schwalm, C.R., Sitch, S., 2014. Modeling the terrestrial biosphere. *Ann. Rev. Environ. Res*., 39, 91-123

Flanner, M.G., Zender, C.S., 2005. Snowpack radiative heating: Influence on Tibetan Plateau climate. *Geophys. Res. Lett*., 32, L06501. doi:10.1029/2004GL022076

Flanner, M.G., Zender, C.S., 2006. Linking snowpack microphysics and albedo evolution. *J. Geophys. Res.*, 111, D12208. doi:10.1029/2005JD006834

Flanner, M.G., Zender, C.S., Randerson, J.T., Rasch, P.J., 2007. Present-day climate forcing and response from black carbon in snow. *J. Geophys. Res.*, 112, D11202. doi:10.1029/2006JD008003

Global Carbon Project (2010) Carbon budget and trends 2009. Available online at: http://www.globalcarbonproject.org/carbonbudget/09/files/GCP2010_CarbonBudget2009.pdf. Accessed May 26, 2011

Harmon, M.E., Bible, K., Ryan, M.G., Shaw, D.C., Chen, H., Klopatek, J., Li, X., 2004. Production, respiration, and overall carbon balance of an old-growth *Pseudotsuga-Tsuga* Forest Ecosystem. *Ecosystems*, 7: 498-512

Harris, P.P., Huntingford, C., Gash, J.H.C., Hodnett, M.G., Cox, P.M., Malhi, Y., Arauijo, A.C., 2004. Calibration of a land-surface model using data from primary forest sites in Amazonia. *Theoretical Applied Climatology*, 78: 27-45

Hayes, T.P., Kinney, J.J.R., Wheeler, N.J.M., 1984. *California surface wind climatology*. California Air Resources Board, Aerometric Data Division, Aerometric Projects and Laboratory Branch, Meteorology Section, Sacramento, California, USA

Humphreys, E.R., Black, T.A., Ethier, G., Drewitt, G., Spittlehouse, D., Jork, E., Nesic, Z., Livingston, N., 2003. Annual and seasonal variability of sensible and latent heat fluxes above a coastal Douglas-fir forest, British Columbia. *Agricultural and Forest Meteorology*, 115, 109-125

Jelalian, A.V., 1992. *Laser Radar Systems*. Artech House, Boston, Massachusetts

Jones, H., Armstrong, D., Blake, R., Bertoldo, N., Cerruti, S., Dibley, V., Doman, J., Grayson, A., Heidecker, K., Hollister, R., Kumamoto, G., MacQueen, D., Nelson, J., Ottaway, H., Paterson, L., Revelli, M., Rosene, C., Terrill, A., Wegrecki, A., Wilson, K., Woollett, J., 2012. *Lawrence Livermore National Laboratory Environmental Report 2011*, UCRL-TR-50027-11, 185p

Kang, S., Running, S.W., Kimball, J.S., Fagre, D.B., Michaelis, A., Peterson, D.L., Halofsky, J.E., Hong, S., 2014. Effects of spatial and temporal climatic variability on terrestrial carbon and water fluxes in the Pacific Northwest, USA. *Environ. Model. Softw*., 51, 228-239

Karipot, A., Leclerc, M.Y., Zhang, G., Martin, T., Starr, G., Hollinger, D., McCaughey, J.H., Hendrey, G.R., 2006. Nocturnal CO2 exchange over a tall forest canopy associate with intermittent low-level jet activity. *Theor. Appl. Climatol*., 85, 243-248

Kobayashi, H., Baldocchi, D., Ryu, Y., Chen, Q., Ma, S., Osuna, J., Ustin, S.L. 2012. Modeling energy and carbon fluxes in a heterogeneous oak woodland: a three-dimensional approach. *Agricultural and Forest Meteorology*, 152, 83-100

Ma, S., Baldocchi, D.D., Xu, L., Hehn, T., 2007. Inter-annual variability in carbon dioxide exchange of an oak/grass savanna and open grassland in California. *Agricultural and Forest Meteorology*, 147, 157-171

Marras, S., Pyles, R.D., Sirca, C., Paw U, K.T., Snyder, R.L., Duce, P., Spano, D., 2011. Evaulation of the Advanced Canopy-Atmosphere-Soil Algorithm (ACASA) model performance over a Mediterranean maquis ecosystem. *Agricultural and Forest Meteorology*, 151: 730-745

Meyers, T., Paw U, K.T., 1986. Testing of a higher-order closure model for modeling airflow within and above plant canopies. *Boundary-Layer Meteor*., 37, 297-311

Moffat, A.M., Papale, D., Reichstein, M., Hollinger, D., Richardson, A.D., Barr, A.G., Beckstein, C., Braswell, B., Churkina, G., Desai, A., Falge, E., Gove, J., Heimann, M., Hui, D., Jarvis, A., Kattge, J., Noormets, A., Stauch, V., 2007. Comprehensive comparison of gap-filling techniques for eddy covariance net carbon fluxes. *Agricultural and Forest Meteorology*, 147: 209-232

Newman, J.F., Bonin, T.A., Klein, P., Wharton, S., Chilson, P.B., 2014. Optimizing lidar scanning strategies for wind energy turbulence measurements. *Proceedings 21st Symposium on Boundary Layers and Turbulence*, Leeds, UK, 9-13 June 2014, American Meteorological Society, Boston, MA, Abstract 17A.5

Niu, G.-Y., Yang, Z.-L., Dickinson, R.E., Goulen, L.E., 2005. A simple TOPMODEL-based runoff parameterization (SIMTOP) for use in global climate models. *J Geophys. Res.*, 110, D21106

Oak Ridge National Laboratory Distributed Active Archive Center (ORNL DAAC), 2013. FLUXNET Maps & Graphics Web Page. Available online [http://fluxnet.ornl.gov/maps-graphics] from ORNL DAAC, Oak Ridge, Tennessee, U.S.A. Accessed October 20, 2014

Olchev, A., Ibrom, A., Ross, T., Falk, U., Rakkibu, G., Radler, K., Grote, S., Kreilein, H., Gravenhorst, G., 2008. A modeling approach for simulation of water and carbon dioxide exchange between multi-species tropical rainforest and the atmosphere. *Ecological Modelling*, 212: 122-130

Papale, D., Valentini, R., 2003. A new assessment of European forests carbon exchanges by eddy fluxes and artificial neural network spatialization. *Global Change Biology*, 9: 525-535

Parker, G.G., Davis, M., Chapotin, S.M., 2002. Canopy light transmittance in Douglas-fir-western-hemlock stands. *Tree Physiology*, 22, 147-157

Paw U, K.T., Gao, W., 1998. Applications of solutions to non-linear energy budget equations. *Agricultural and Forest Meteorology*, 43, 121-145

Paw U, K.T., Baldocchi, D., Meyers, T.P., and Wilson, K.B., 2000. Correction of eddy covariance measurements incorporating both advective effects and density fluxes. *Boundary Layer Meteorology*, 91, 487-511.

Peña, A., Hasager, C.B., Gryning, S.-E., Courtney, M., Antoniou, I., Mikkelsen, T., 2009. Offshore wind profiling using light detection and ranging measurements. *Wind Energy*, 12, 105-124

Pichugina, Y.L., Banta, R.M., Kelley, N.D., Jonkman, B.J., Tucker, S.C., Newsom, R.K., Brewer, W.A., 2008. Horizontal velocity and variance measurements in the stable boundary layer using Doppler lidar: sensitivity to averaging procedures. *J. Atmos. Oceanic Technol*., 25, 1307-1327

Pyles, R.D., Weare, B.C., Paw U, K.T., 2000. The UCD Advanced-Canopy-Atmosphere-Soil Algorithm (ACASA): Comparisons with observations from different climate and vegetation regimes. *Quarterly Journal of the Royal Meteorological Society*, 126: 2951-2980

Pyles, R.D., Paw U, K.T., Falk, M., 2004. Directional wind shear within an old-growth temperate rainforest: observations and model results. *Agricultural and Forest Meteorology*, 125, 19-31

Running, S.W., Hunt, E.R., 1993. Generalization of a forest ecosystem process model for other biomes, Biome-BGC, and an application for global-scale models. *In: Scaling Physiological Processes: Leaf to Globe*, 141-158p

Ryu, Y., Sonnentag, O., Nilson, T., Vargas, R., Kobayashi, H., Wenk, R., Baldocchi, D., 2010. How to quantify tree leaf area index in an open savanna ecosystem: a multi-instrument and multi-model approach. *Agricultural and Forest Meteorology*, 150, 63-76

Sathe, A., Mann, J., Gottschall, J., Courtney, M.S., 2011. Can wind lidars measure turbulence? *J Atmos. Oceanic Technol*., 28, 853-868

Shaw, D.C., Franklin, J.F., Bible, K., Klopatek, J., Freeman, E., Greene, S., Parker, G.G., 2004. Ecological setting of the Wind River old-growth forest. *Ecosystems*, 7, 427-439

Slinger, C., Harris, M., 2012. Introduction to continuous-wave Doppler lidar. Technical Report, 32p

Smirnova, T.G., Brown, J.M., Benjamin, S.G., Kim, D., 2000. Parameterization of cold-season processes in the MAPS land-surface scheme. *J Geophys. Res*., 105, 4077-4086

Smith, D.A., Harris, M., Coffey, A.S., Mikkelsen, T., Jørgensen, H.E., Mann, J., Danielian, R., 2006. Wind lidar evaluation at the Danish wind test site in Høvsøre. *Wind Energy*, 9, 87-93

Strauch, R.G., Merritt, D.A., Moran, K.P., Earnshaw, K.B., De Kamp, D.V., 1984. The Colorado Wind-Profiling Network. *J Atmos. Oceanic Technol*., 1, 37-49

Thomas, C.K., Martin, J.G., Law, B.E., Davis, K., 2013. Toward biologically meaningful net carbon exchange estimates for tall, dense canopies: multi-level eddy covariance observations and canopy coupling regimes in a mature Douglas-fir forest in Oregon. *Agricultural and Forest Meteorology*, 173, 14-27

Thomas, S.C., Winner, W.E., 2000. Leaf area index of an old-growth Douglas-fir forest estimated from direct structural measurements in the canopy. *Can J. For. Res.*, 30, 1922–1930

Thornton, P.E., Law, B.E., Gholz, H.L., Clark, K.L., Falge, E., Ellsworth, D.S., Goldstein, A.H., Monson, R.K., Hollinger, D., Falk, M., 2002. Modeling and measuring the effects of disturbance history and climate on carbon and water budgets in evergreen needleleaf forests. *Agricultural and Forest Meteorology*, 113, 185-222

van Gorsel, E., Delpierre, N., Leuning, R., Black, A., Munger, J.W., Wofsy, S., Aubinet, M., Feigenwinter, C., Wharton, S. *et al.*, 2009. Estimating nocturnal ecosystem respiration from the vertical flux and change in storage of CO_2. *Agricultural and Forest Meteorology*, 149, 1919-1930

Vickers, D., Irvine, J., Martin, J.G., Law, B.E., 2012. Nocturnal subcanopy flow regimes and missing carbon dioxide. *Agricultural and Forest Meteorology*, 152, 101-108

Wagner, R, Mikkelsen, T., Courtney, M., 2009. Investigation of turbulence measurements with a continuous wave, conically-scanning lidar. Risø DTU Tech. Rep. Risø-R-1682(EN), 22 p

Webb, E.K., Pearman, G.I., Launing, R., 1980, Correction of flux measurements for density effects due to heat and water vapour transfer. *Q. J. Royal Meteorol.* Soc., 106, 85-10

Wharton, S., Schroeder, M., Paw U, K.T., Falk, M., Bible, K., 2009a. Turbulence considerations for comparing ecosystem exchange over old-growth and clear-cut stands for limited fetch and complex canopy flow conditions. *Agricultural and Forest Meteorology*, 149, 1477-1490

Wharton, S., Schroeder, M., Bible, K., Falk, M., Paw U, K.T., 2009b. Stand-level gas-exchange responses to seasonal drought in very young versus old Douglas-fir forests of the Pacific Northwest, USA. *Tree Physiology* 29: 959-974

Wharton, S., Falk, M., Bible, K., Schroeder, M., Paw U, K.T., 2012. Old-growth CO_2 flux measurements reveal high sensitivity to climate anomalies across seasonal, annual and decadal time scales. *Agricultural and Forest Meteorology* 161: 1-14

Whiteman, C.D., Zhong, S.-Y, 2008. Downslope flows on a low-angle slope and their interactions with valley inversions. Part 1: Observations. *J Applied Meteor. Climatol*., 47, 2023-2038

Yi, C., Monson, R.K., Zhai, Z., Anderson, D., Lamb, B., Allwine, G., Turnipseed, A., Burns, S.P., 2005. Modeling and measuring the nocturnal drainage flow in high-elevation, subalpine forest in complex terrain. *J Geophysical Research*, 110: D22303, doi:10.1029/2005JD006282

Xu, L., Baldocchi, D., 2003. Seasonal trend of photosynthetic parameters and stomatal conductance of blue oak (*Quercus douglasii*) under prolonged summer drought and high temperature. *Tree Physiology*, 23, 865-877

Xu, L., Pyles, R.D., Paw U, K.T., Chen, S.H., Monier, E., 2014. Coupling the highly complexity land surface model ACASA to the mesoscale model WRF. *Geosci. Model Dev. Discuss.*, 7, 2829-2875